Molecular Biology of the Cell
Vol. 17, 607–622, February 2006

The Inositol Polyphosphate 5-Phosphatase, PIPP, Is a Novel Regulator of Phosphoinositide 3-Kinase-dependent Neurite Elongation

Lisa M. Ooms,* Clare G. Fedele,* Megan V. Astle,* Ivan Ivetac,* Vanessa Cheung,* Richard B. Pearson,† Meredith J. Layton,‡ Ariel Forrai,* Harshal H. Nandurkar,* and Christina A. Mitchell*

*Department of Biochemistry and Molecular Biology, Monash University, Clayton 3800, Victoria, Australia; †Trescowthick Research Laboratories, Peter MacCallum Cancer Institute, Melbourne 8006, Victoria, Australia; and ‡Ludwig Institute of Medical Research, Joint Proteomics Research Laboratory, Parkville 3050, Victoria, Australia

Submitted May 31, 2005; Revised October 7, 2005; Accepted November 2, 2005
Monitoring Editor: John York

The spatial activation of phosphoinositide 3-kinase (PI3-kinase) signaling at the axon growth cone generates phosphatidylinositol 3,4,5 trisphosphate (PtdIns(3,4,5)P_3), which localizes and facilitates Akt activation and stimulates GSK-3β inactivation, promoting microtubule polymerization and axon elongation. However, the molecular mechanisms that govern the spatial down-regulation of PtdIns(3,4,5)P_3 signaling at the growth cone remain undetermined. The inositol polyphosphate 5-phosphatases (5-phosphatase) hydrolyze the 5-position phosphate from phosphatidylinositol 4,5 bisphosphate (PtdIns(4,5)P_2) and/or PtdIns(3,4,5)P_3. We demonstrate here that PIPP, an uncharacterized 5-phosphatase, hydrolyzes PtdIns(3,4,5)P_3 forming PtdIns(3,4)P_2, decreasing Ser473-Akt phosphorylation. PIPP is expressed in PC12 cells, localizing to the plasma membrane of undifferentiated cells and the neurite shaft and growth cone of NGF-differentiated neurites. Overexpression of wild-type, but not catalytically inactive PIPP, in PC12 cells inhibited neurite elongation. Targeted depletion of PIPP using RNA interference (RNAi) resulted in enhanced neurite differentiation, associated with neurite hyperelongation. Inhibition of PI3-kinase activity prevented neurite hyperelongation in PIPP-deficient cells. PIPP targeted-depletion resulted in increased phospho-Ser473-Akt and phospho-Ser9-GSK-3β, specifically at the neurite growth cone, and accumulation of PtdIns(3,4,5)P_3 at this site, associated with enhanced microtubule polymerization in the neurite shaft. PIPP therefore inhibits PI3-kinase-dependent neurite elongation in PC12 cells, via regulation of the spatial distribution of phospho-Ser473-Akt and phospho-Ser9-GSK-3β signaling.

INTRODUCTION

Neurite extension and retraction are critical events in the formation and integration of neuronal networks (Bernstein and Lichtman, 1999; Lee and Van Vactor, 2003). Neurite extension is governed by both actin cytoskeletal and microtubular dynamics (Tanaka and Sabry, 1995; Skaper *et al.*, 2001; Dickson, 2002); however, the specific intracellular signaling pathways that stimulate or inhibit neurite extension have not been comprehensively delineated. Neurons integrate extracellular signals to regulate axon initiation and guidance at growth cones, which are localized to the tips of growing axons (see Baas and Luo, 2001 for a review). Actin polymerization at the leading edge of the growth cone and subsequent microtubule polymerization and bundling facilitate the formation and elongation of axons (Gordon-Weeks, 1991).

A significant signaling pathway that stimulates neurite outgrowth and differentiation is mediated by PI3-kinase signaling, which facilitates both turning and branching at the growth cone or axon shaft in response to neurotrophin stimuli (Gallo and Letourneau, 1998; Ming *et al.*, 1999). Nerve growth factor (NGF) stimulates the activation of PI3-kinase which generates phosphatidylinositol 3,4,5 trisphosphate (PtdIns(3,4,5)P_3; Carter and Downes, 1992; Raffioni and Bradshaw, 1992; Soltoff *et al.*, 1992). This phosphoinositide signal recruits cytosolic effectors including the serine threonine kinase Akt, integrin-linked kinase (ILK) and glycogen synthase kinase 3β (GSK-3β), facilitating their phosphorylation and/or inactivation thereby promoting neuronal survival and differentiation, actin dynamics, and microtubule polymerization leading to axon elongation (Cantley, 2002; Rodgers and Theibert, 2002; Zhou and Snider, 2005). In differentiating neurons activation of PI3-kinase may occur at the growth cone, as shown by the concentration of its down-stream effectors phospho-Ser473-Akt and phospho-Ser9-GSK-3β at this site (Shi *et al.*, 2003; Zhou *et al.*, 2004; Jiang *et al.*, 2005).

This article was published online ahead of print in *MBC in Press* (http://www.molbiolcell.org/cgi/doi/10.1091/mbc.E05–05–0469) on November 9, 2005.

Address correspondence to: Christina Mitchell (Christina.Mitchell@med.monash.edu.au).

Abbreviations used: 5-phosphatase, inositol polyphosphate 5-phosphatase; GSK-3β, glycogen synthase kinase 3β; NGF, nerve growth factor; PIPP, proline-rich inositol polyphosphate 5-phosphatase; PI3-kinase, phosphoinositide 3-kinase; PtdIns, phosphatidylinositol; RNAi, RNA interference.

The rat pheochromocytoma cell line, PC12, has been used extensively as a model system to investigate NGF-dependent neuronal survival and differentiation. NGF stimulates differentiation of PC12 cells into neuronlike cells with processes that extend to form long neurites (Greene and Tischler, 1976). Treatment of PC12 cells with the PI3-kinase inhibitors wortmannin or LY294002 inhibits neurite initiation and extension and induces the collapse of mature neurites in differentiated cells (Jackson *et al.*, 1996). In contrast, expression of constitutively active PI3-kinase stimulates the formation of neuritelike processes that lack F-actin and GAP43 at the growth cone, associated with increased microtubule bundling (Kobayashi *et al.*, 1997). PC12 cells expressing a constitutively active form of the serine/threonine kinase Akt extend fewer, longer neurites, with less branches in response to NGF stimulation (Higuchi *et al.*, 2003). In contrast, expression of a dominant-negative form of Akt results in increased numbers of neurite processes and branch points (Bang *et al.*, 2001; Higuchi *et al.*, 2003).

The inositol polyphosphate 5-phosphatases (5-phosphatases) are a family of signal-modifying enzymes comprising 10 mammalian and 4 yeast members (Mitchell *et al.*, 2002). 5-phosphatases hydrolyze the 5-position phosphate from PtdIns(3,4,5)P_3 and/or PtdIns(4,5)P_2 forming PtdIns(3,4)P_2 and PtdIns(4)P, respectively. Gene-targeted deletion of specific 5-phosphatases in mice has revealed nonredundant functions for these enzymes in hematopoietic cell proliferation, synaptic vesicle recycling, insulin signaling, endocytosis, and actin polymerization (Helgason *et al.*, 1998; Cremona *et al.*, 1999; Kim *et al.*, 1999; Clement *et al.*, 2001; Hellsten *et al.*, 2002; Sleeman *et al.*, 2005). The proline-rich inositol polyphosphate 5-phosphatase (PIPP) is a relatively uncharacterized 5-phosphatase that hydrolyzes PtdIns(4,5)P_2, Ins(1,4,5)P_3, and Ins(1,3,4,5)P_4 (Mochizuki and Takenawa, 1999); however, its ability to hydrolyze PtdIns(3,4,5)P_3 and regulate PI3-kinase signaling has not been reported thus far. Recombinant PIPP is constitutively associated with the plasma membrane, mediated by its C-terminal SKICH domain (Gurung *et al.*, 2003). PIPP is expressed in a number of tissues including brain, heart, kidney, stomach, small intestine, and lung (Mochizuki and Takenawa, 1999), but the specific functional role of PIPP remains unexplored.

In the study reported here, we have identified PIPP as a novel regulator of PI3-kinase signaling. We demonstrate that PIPP hydrolyzes PtdIns(3,4,5)P_3 and regulates Akt phosphorylation. PIPP is expressed in PC12 cells, localizing to the plasma membrane of undifferentiated cells. In NGF-differentiated cells, PIPP is concentrated at the neurite growth cone. We have overexpressed PIPP and utilized targeted depletion of PIPP by RNA interference (RNAi) in PC12 cells to investigate the function of PIPP in neuronal differentiation. Overexpression of PIPP had no effect on neurite initiation, but neurite extension was significantly impaired. Decreased PIPP protein expression, as a consequence of RNAi, was associated with significant hyperelongation of NGF differentiated neurites. Our results suggest that these phenotypes could be mediated, at least in part, by PIPP-dependant regulation of the spatial distribution of PI3-kinase-dependent Akt and GSK-3β phosphorylation at the growth cone. Collectively, these results identify that PIPP functions as a negative regulator of PI3-kinase signaling events that promote neurite elongation.

MATERIALS AND METHODS

Restriction and DNA-modifying enzymes were from Fermentas (Burlington, Canada), New England Biolabs (Beverly, MA), or Promega (Madison, WI). GFP/PH-ARNO and PH/PLCδ1-GFP were a gift from Dr. Tamas Balla (National Institutes of Health), GFP-PH/TAPP1 was a gift from Dr. Dario Alessi (University of Dundee, United Kingdom), pCGN and pEFBOS vectors were from Dr. Tony Tiganis (Monash University, Australia). Texas Red phalloidin was from Molecular Probes (Eugene, OR). GSK-3β, phospho-GSK-3β, Akt and phospho-Akt antibodies and an immunohistochemistry-specific phospho-Akt antibody were from Cell Signaling (Beverly, MA) and a monoclonal FLAG tag antibody was from Sigma (St. Louis, MO). Monoclonal antibodies to hemagglutinin (HA) were from Covance (Richmond, CA) and polyclonal antibodies were from Upstate Biotechnology (Waltham, MA). The β-tubulin antibody was from Zymed (San Francisco, CA) and an actin-specific antibody was from Lab Vision (Fremont, CA). [γ-^{32}P]ATP was from NEN Life Science Products (Boston, MA). Synthetic peptides were obtained from Chiron Mimotopes (Melbourne, Australia) and oligonucleotides were obtained either from Geneworks (Adelaide, Australia) or from Micromon (Monash University, Australia). Cell lines were from the American Type Culture Collection (Manassas, VA). All other reagents were from Sigma (St. Louis, MO) unless otherwise stated.

Cloning of Full-length Murine PIPP

The full-length mouse homolog of the proline-rich PIPP was cloned by using a human EST (U45975), encoding a partial human inositol polyphosphate 5-phosphatase, to screen a mouse heart cDNA library. A partial 3185-base pair clone was obtained that contained a 3′ polyadenylation signal, but lacked an initiating methionine. Subsequent rapid amplification of 5′ ends (RACE) using mouse heart mRNA as a template and the primers GGCCACGCGTCGACTAGTACGGGGGGGGGIIG and ACCTCTCCACCAAGGGCCCAAGCTT identified a further 193 base pairs of sequence upstream, which contained an in-frame methionine residue. Products from this PCR were then used as a template for nested PCR using the primers CUACUACUACUAGGCCACGCGTCGACTAGTAC and TCCGTCCTAACTCCAACTTCTA. The two fragments were ligated using a unique *Hin*dIII site present in the overlapping region to obtain a full-length clone. Although no upstream in-frame stop codon was identified, the predicted initiating methionine aligns exactly with the corresponding residue in the reported rat PIPP homolog (Mochizuki and Takenawa, 1999). The predicted mouse PIPP amino acid sequence shares 94% amino acid identity with rat PIPP and contains extensive proline-rich domains at the N- and C-termini, and a central 5-phosphatase catalytic domain followed by a SKICH domain (Figure 1A; Gurung *et al.*, 2003).

To generate HA or FLAG tag fusion constructs, the full-length PIPP cDNA was amplified by PCR and subcloned into the *Xba*I site of pCGN in-frame with the N-terminal HA tag or the *Mlu*I site of pEFBOS in-frame with the N-terminal FLAG tag. Catalytically inactive PIPP was generated by mutating histidine 557 within the PIPP sequence to alanine. PIPP^{SKICH}, encoding aa 767–836 of PIPP, was cloned into pCGN in-frame with the N-terminal HA tag as previously described (Gurung *et al.*, 2003).

Production of a PIPP-specific Anti-peptide Antibody

An anti-peptide antibody was raised in New Zealand White rabbits to a synthetic peptide conjugated to diphtheria toxoid. The peptide corresponded to a unique sequence in the SKICH domain of PIPP (^{790}KHEDVDGNTYQVTFSEEC^{805}). Anti-peptide antibodies were affinity-purified by chromatography using the peptide coupled to thiopropyl-Sepharose according to the manufacturer's instructions. Peptide absorbed antibody was generated by two sequential incubations of immune serum with the immune peptide coupled to thiopropyl-Sepharose.

Transient Transfection

COS-1 cells were maintained in DMEM supplemented with 10% newborn calf serum, 2 mM L-glutamine, 100 U/ml penicillin, and 0.1% streptomycin. Cells were transiently transfected by the dextran/chloroquine method. Dextran/chloroquine, 200 μl, (400 μg/ml dextran, 100 μM chloroquine), 5 μg DNA, and 5 ml serum-free DMEM was added to a 50% confluent 10-cm dish and incubated for 2 h at 37°C with 5% CO_2. Cells were treated in 10% dimethyl sulfoxide/phosphate-buffered saline (PBS) for 2 min at room temperature and then incubated in DMEM with 10% newborn calf serum for 2 d at 37°C with 5% CO_2. For EGF stimulation, cells were incubated for 16 h in serum-free medium and then 100 ng/ml EGF was added and cells were incubated at 37°C for the indicated times.

PC12 cells were maintained in DMEM containing 10% fetal calf serum (FCS), 5% horse serum, 2 mM L-glutamine, 100 U/ml penicillin, and 0.1% streptomycin. Cells were transiently transfected by electroporation in 200 μl of the above medium. A 50 μl DNA mix containing 5 μg DNA, 0.15 M NaCl was added to the cells and then the mix was electroporated at 0.2 kV, 0.975 μF. The cells were added to 8 ml of the above medium and incubated at 37°C with 5% CO_2 for 2 d. For immunofluorescence PC12 cells were plated onto 0.01% poly-L-lysine-coated coverslips. For differentiation, cells were incubated in DMEM containing 1% horse serum and 100 ng/ml NGF for the indicated times. To inhibit PI3-kinase, cells were treated with 100 nM wortmannin or 50 μM LY294002 on either day 0 or day 1 of NGF stimulation then allowed to differentiate for a total of 3 d. Fresh wortmannin was added every 24 h because the inhibitor is unstable in tissue culture.

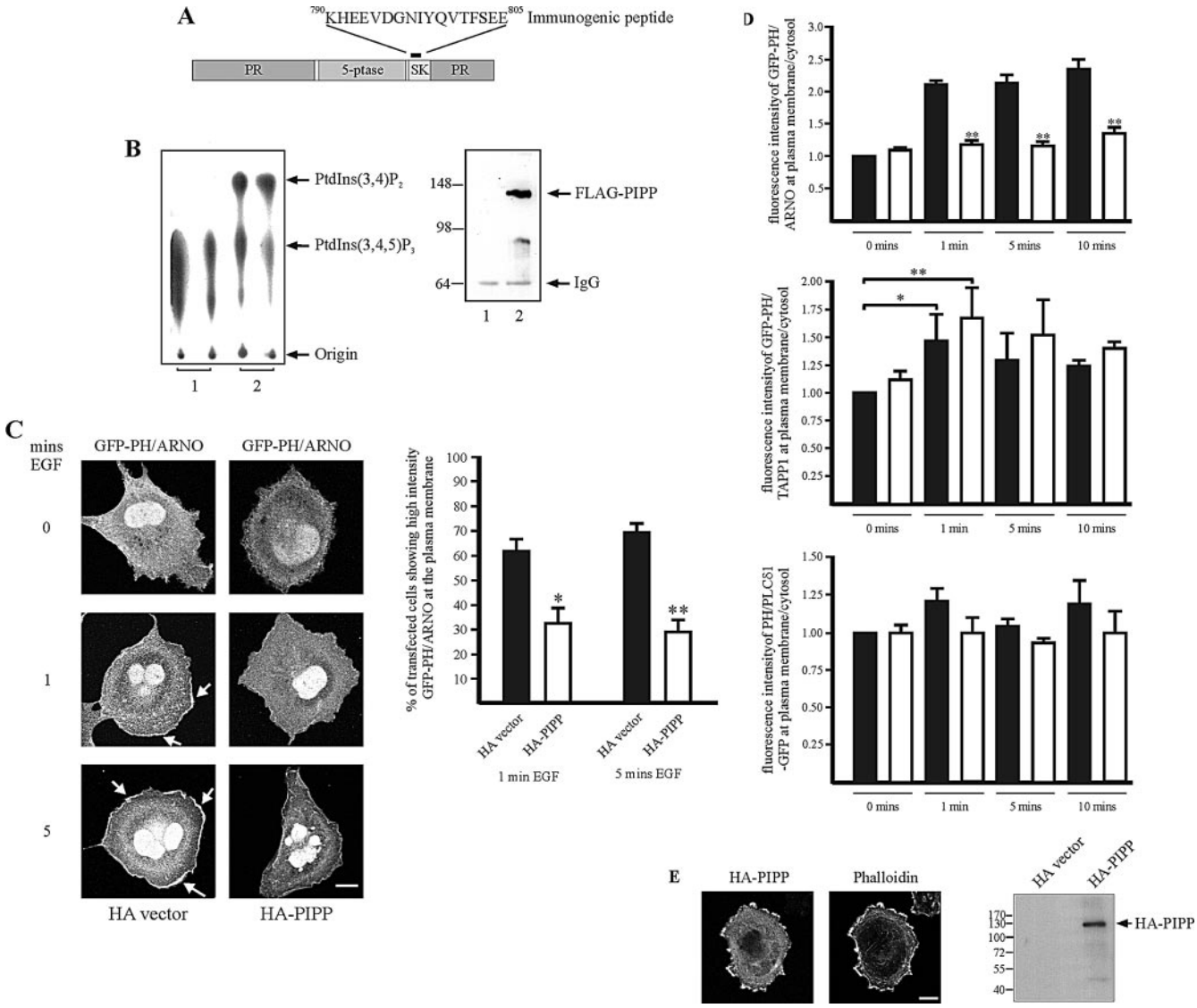

Figure 1. PIPP hydrolyzes PtdIns(3,4,5)P_3. (A) Diagram of the domains in the PIPP sequence including proline-rich domain (PR), 5-phosphatase domain (5-ptase), and SKICH domain (SK). The peptide sequence used as an immunogen to generate a PIPP-specific peptide antibody is indicated. (B) Plasmids encoding FLAG-tagged PIPP or FLAG-vector were transiently transfected into COS-1 cells. Cell lysates derived from transfected cells were immunoprecipitated with FLAG antibodies. Duplicate immunoprecipitates derived from FLAG-vector (lane 1) or FLAG-PIPP-expressing cells (lane 2) were assayed for PtdIns([^{32}P]-3,4,5)P_3 5-phosphatase activity, and lipid products were analyzed by TLC chromatography (Kong *et al.,* 2000). The TLC shown is representative of five similar experiments. The origin and the migration of PtdIns(3,4)P_2 and PtdIns(3,4,5)P_3 are indicated on the right. Parallel FLAG-immunoprecipitates from FLAG-vector (lane 1) or FLAG-PIPP-expressing cells (lane 2) were immunoblotted with FLAG antibodies to confirm immunoprecipitation of FLAG-PIPP. The migration of molecular-weight markers (kDa) is shown on the left. (C) COS-1 cells were transiently cotransfected with plasmids encoding GFP-PH/ARNO and either HA alone (■) or HA-PIPP (□). Cells were serum-starved, or starved and then stimulated with 100 ng/ml EGF for 1 or 5 min as indicated and stained with HA antibodies to identify cotransfected cells (unpublished data). Transfected cells were scored for GFP-PH/ARNO fluorescence at the plasma membrane (see arrows) using confocal microscopy. Representative images are shown. Bars represent the mean ± SEM of three separate transfections in which 35 cells were scored for GFP-PH/ARNO plasma membrane fluorescence (>100 cells scored per construct; * $p < 0.05$, ** $p < 0.01$). Scale bar, 20 μm. D. COS-1 cells were transiently cotransfected with plasmids encoding HA alone (■) or HA-tagged PIPP (□), with either GFP-PH/ARNO (top), or GFP-PH/TAPP1 (middle), or PH/PLCδ1-GFP (bottom). Cells were serum-starved, or starved overnight and then stimulated with 100 ng/ml EGF for 1, 5, or 10 min and stained with HA antibodies to identify HA-PIPP expressing cells (unpublished data). The fluorescence intensity of the GFP-phosphoinositide biosensor at the plasma membrane, as a ratio of that detected in the cytosol, was determined using Image J software by measuring the average pixel intensity within three areas of ~150 pixels each on the plasma membrane and three areas of 500 pixels each in the cytosol of the same cell. Bars, the mean ± SEM of four (GFP-PH/ARNO, >34 cells scored) or three (GFP-TAPP1, >28 cells scored and PH/PLCδ1-GFP, >24 cells scored) independent transfections for each construct. (* $p < 0.05$, ** $p < 0.01$). (E) COS-1 cells were transiently transfected with a plasmid encoding HA-PIPP, serum-starved overnight (unpublished data) and stimulated with serum, fixed, and costained with an antibody against the HA-tag and Texas Red phalloidin, or cell lysates were immunoblotted with an HA antibody. Molecular-weight markers (kDa) are indicated on the left. The migration of HA-PIPP is indicated by the arrow. Scale bar, 20 μm.

For transfection of differentiated PC12 cells, the cells were grown overnight on 0.01% poly-L-lysine-coated coverslips and treated with 100 ng/ml NGF for 2 d. Cells were transfected with 1 μg DNA using 1 μl Lipofectamine 2000 (Invitrogen, Carlsbad, CA) according to the manufacturer's instructions and then treated with NGF for a further 24 h.

Western Blotting

Cells were washed two times with PBS and then scraped from the dish in 500 μl lysis buffer (20 mM Tris, pH 7.4, 150 mM NaCl, 1 mM phenylmethylsulfonyl fluoride [PMSF], 1 mM benzamidine, 0.2 μg/ml aprotinin, 0.2 μg/ml leupeptin). Lysates were sonicated for 30 s, and then 20–50 μg protein was separated by 10% SDS-PAGE, transferred to PVDF, and blotted with the appropriate antibodies. Relative protein levels in each sample were determined by densitometry.

PtdIns(3,4,5)P_3 Assays

COS-1 cells were transiently transfected with pEFBOS or PIPP-pEFBOS. Forty-eight hours after transfection, cells were harvested in 0.5 ml extraction buffer (20 mM Tris, pH 8, 200 mM NaCl, 10% sucrose, 1% Triton X-100, 1 mM PMSF, 0.2 μg/ml aprotinin, 0.2 μg/ml leupeptin) and then incubated at 4°C for 2 h with gentle agitation. Samples were centrifuged at 13,000 $\times$ *g* for 10 min to obtain the Triton-soluble supernatant. Monoclonal FLAG antibody (2 μl), anti-mouse linker antibody (2 μl), and 50% protein A Sepharose slurry (60 μl) were added to the supernatant and the mix was incubated at 4°C overnight with gentle agitation. The pellets were washed six times with cold PBS, and then PtdIns(3,4,5)P_3 assays were performed on the immunoprecipitates. The PtdIns([^{32}P]3,4,5)P_3 substrate was prepared as previously described (Kong *et al.*, 2000). Phosphatidylserine (12.5 μg) and PtdIns(4,5)P_2 (32.5 μg) were mixed and dried under nitrogen, then resuspended in 200 μl of lipid resuspension buffer (20 mM HEPES, pH 7.5, 1 mM $MgCl_2$, 1 mM EGTA), and sonicated for 5 min. This suspension, 50 μl, was added to 5 μl 20$\times$ kinase buffer (400 mM HEPES, pH 7.5, 100 mM $MgCl_2$, 20 mM EGTA), 20 μl [γ-^{32}P]ATP (2 mCi, 3000 mCi/mmol), 5 nmol unlabeled ATP, and 1 μg affinity-purified recombinant PI3-kinase in a reaction volume of 100 μl and incubated overnight at room temperature. The reaction was terminated by the addition of 1 M HCl, and following the addition of 5 μg of phosphatidylserine, the lipids were extracted with 200 μl chloroform/methanol (1:1) and 500 μl 2 M KCl saturated with chloroform, dried under nitrogen, and resuspended in 300 μl lipid resuspension buffer. PtdIns(3,4,5)P_3 5-phosphatase assays were performed on immunoprecipitates by the addition of 4 μl 20$\times$ kinase buffer and 80 μl PtdIns([^{32}P]3,4,5)P_3 substrate. Reactions were incubated at 37°C for 30 min, and then lipids were extracted as above and analyzed by TLC. ^{32}P-labeled phosphoinositides were extracted from the TLC plate and verified by deacylation and HPLC analysis as described (Kong *et al.*, 2000).

PtdIns(3,5)P_2 Assays

PtdIns([^{32}P]3,5)P_2 was prepared as described for PtdIns([^{32}P]3,4,5)P_3 except that 40 μg PtdIns(5)P was used in the PI3-kinase assays. PtdIns(3,5)P_2 5-phosphatase assays were performed as for PtdIns(3,4,5)P_3 5-phosphatase assays and analyzed by TLC as previously described (Kong *et al.*, 2000).

Assessment of Plasma Membrane Levels of PtdIns(4,5)P_2, PtdIns(3,4,5)P_3, and PtdIns(3,4)P_2

COS-1 cells were transiently cotransfected with 10 μg of either pCGN or PIPP-pCGN together with 5 μg of either GFP-PH/ARNO, PH/PLCδ1-GFP, or GFP-PH/TAPP1 with dextran/chloroquine as above. One day after transfection cells were serum-starved in serum-free DMEM for 16 h at 37°C. Cells were stimulated with 100 ng/ml EGF for 0, 1, 5, or 10 min and then fixed in 3% paraformaldehyde/PBS for 20 min and permeabilized in 0.1% Triton X-100/PBS for 2 min. Cells were blocked with 1% BSA/PBS for 15 min before being incubated with a monoclonal HA antibody followed by an α-mouse Alexa 594 secondary antibody for 1 h each. Cells were analyzed with a Leica TCS-NT confocal microscope (Heidelberg, Germany) with an Ar-Kr triple-line laser at Monash MicroImaging (Monash University, Australia). Relative fluorescence intensity of the phosphoinositide biosensors at the plasma membrane was measured using the Image J program (version 1.34; NIH) as a ratio of the average pixel intensity within three areas of intense GFP accumulation on the plasma membrane relative to the average pixel intensity of three areas of the cytosol of the same cell.

Assessment of Phospho-Ser473-Akt or Phospho-Ser9-GSK-3β by Immunoblot Analysis

COS-1 cells were transiently transfected with 5 μg of either pCGN or PIPP-pCGN by the dextran/chloroquine method as above. One day after transfection the media was replaced with serum-free DMEM, and the cells were incubated for 16 h at 37°C. Cells were stimulated with 100 ng/ml EGF for 0, 1, 5, or 10 min at 37°C and then placed on ice and washed 2$\times$ with ice-cold PBS before being scraped from the dish in 500 μl lysis buffer (20 mM Tris, pH 7.4, 150 mM NaCl, 1 mM PMSF, 1 mM benzamidine, 0.2 μg/ml aprotinin, 0.2 μg/ml leupeptin, 1 mM sodium vanadate). Lysates were sonicated for 30 s, and then 50 μg protein was separated by 10% SDS-PAGE and transferred to nitrocellulose membranes. Blots were probed with polyclonal antibodies specific for phospho-Ser473-Akt, phospho-Ser9-GSK-3β, or phospho-Thr202/Tyr204-p44/42 (Erk1/2) followed by β-tubulin or actin as a loading control according to manufacturer's instructions. Relative levels of phosphorylated proteins in each sample were determined by densitometry.

For analysis in PC12 cells, after 3-d NGF stimulation cell lysates were harvested as for COS-1 cells and 50 μg of protein was immunoblotted for phospho-Ser473-Akt or total Akt protein, or phospho-Ser9-GSK-3β and total GSK-3β protein using specific antibodies. Phospho-Ser473-Akt or phospho-Ser9-GSK-3β immunoreactive polypeptides were analyzed by densitometry and quantitated relative to total Akt or GSK-3β protein respectively.

Generation of PIPP RNAi Clones

Stable cell lines underexpressing PIPP and scrambled control clones were generated using the psiRNA-hH1neo kit from InvivoGen (San Diego, CA). The following oligonucleotide pairs were annealed and ligated into the *Bbs*I site of the psiRNA-hH1neo vector according to the manufacturer's instructions to generate PIPP-psiRNA-hH1neo and scrambled-psiRNA-hH1neo. (PIPP sense: tccc**aacttccgcattgagagctat***ttcaagaga***atagctctcaatgcggaagt**tt; PIPP antisense: caaaa**aacttccgcattgaga**gctat*tctcttgaa***atagctctcaatgcggaagtt;** Scrambled sense: tccc**aactcatcgagactatgtgct***ttcaagaga***agcacatagtctcgatgagt**tt; Scrambled antisense: caaaa**aactcatcgagactatgtgct***tctcttgaa***agcacatagtctcgatgagtt;** PIPP-specific or scrambled equivalent sequences are in bold, and loop sequences are in italics). The nucleotide sequence of the constructs was confirmed by dideoxy sequencing. Constructs were transfected into PC12 cells as described above, and clones were selected in DMEM + 10% FCS, 5% horse serum, 0.9 mg/ml G418. Individual clones were maintained in DMEM + 10% FCS, 5% horse serum, 0.5 mg/ml G418 and then transferred to DMEM + 10% FCS, 5% horse serum before each experiment.

Indirect Immunofluorescence

Cells were fixed in 3% paraformaldehyde/PBS for 20 min then permeabilized in 0.1% Triton X-100/PBS for 2 min. After fixation, cells were washed three times with PBS and blocked with 1% BSA/PBS for 15 min. Cells were incubated with primary and then secondary antibodies as indicated for 1 h each and then analyzed with a Leica TCS-NT confocal microscope with an Ar-Kr triple-line laser at Monash MicroImaging.

Assessment of Phospho-Ser473-Akt or Phospho-Ser9-GSK-3β by Immunofluorescence

PC12 cells were grown on 0.01% poly-L-lysine-coated coverslips and stimulated for 3 d with 100 ng/ml NGF. For immunofluorescence with Akt antibodies, cells were fixed with 100% methanol at $-$20°C for 5 min, washed three times with PBS and blocked in 1% BSA/PBS for 15 min. Cells were incubated with an immunohistochemistry-specific polyclonal phospho-Ser473-Akt antibody for 8 h or total Akt antibody for 1 h followed by an α-rabbit Alexa 488 secondary antibody for 1 h. For immunofluorescence with GSK-3β antibodies, cells were fixed in 3% paraformaldehyde/PBS for 20 min, permeabilized in 0.1% Triton X-100/PBS for 2 min, washed three times with PBS and blocked in 1% BSA/PBS for 15 min. Cells were incubated with polyclonal phospho-Ser9-GSK-3β or total GSK-3β antibodies for 1 h followed by α-rabbit Alexa 488 secondary antibodies for 1 h. Cells were imaged with a Leica TCS-NT confocal microscope with an Ar-Kr-triple-line laser at the same laser attenuation. Fluorescence intensity was measured as the average pixel intensity within a box of defined size drawn on the neurite shaft or growth cone using the Image J program.

Assessment of PtdIns(3,4,5)P_3 in RNAi Clones by Immunofluorescence

PC12 cells were grown on 0.01% poly-L-lysine-coated coverslips and differentiated with 100 ng/ml NGF in DMEM containing 1% horse serum for a total of 3 d. Forty-eight hours after the addition of NGF, cells were transfected with 1 μg GFP-PH/ARNO using 1 μl Lipofectamine 2000 (Invitrogen) according to manufacturer's instructions and incubated for 24 h in the presence of 100 ng/ml NGF. Cells were fixed in 3% paraformaldehyde in PBS for 20 min and then analyzed with a Leica TCS-NT confocal microscope with an Ar-Kr triple-line laser. Relative fluorescence intensity of GFP-PH/ARNO in the growth cone was measured using the Image J program as a ratio of the average pixel intensity of the most intense region of fluorescence in the growth cone, compared with the average pixel intensity of three areas of the cytosol of the same cell.

Indirect Immunofluorescence of Polymerized Tubulin

Tubulin monomers were extracted and cells were fixed as previously described (He *et al.*, 2002) by incubation in 60 mM 1,4-piperazinediethanesulfonic acid, 25 mM HEPES, 10 mM EGTA, 2 mM $MgCl_2$, pH 6.9, 4% paraformaldehyde, 0.15% glutaraldehyde, 0.2% Triton X-100 for 15 min. After fixation, cells were washed three times with PBS and blocked with 1%

BSA/PBS for 15 min. Cells were incubated with a monoclonal β-tubulin antibody followed by an α-mouse Alexa 488 secondary antibody for 1 h each and then analyzed with a Leica TCS-NT confocal microscope with an Ar-Kr triple-line laser at Monash MicroImaging.

Image Analysis

Image analysis was performed using the public domain Image J software (Abramoff *et al.*, 2004). Laser attenuation settings were kept the same for all images in individual experiments where fluorescence intensity was compared. Fluorescence intensity was measured as the average pixel intensity within a box of defined size drawn on the neurite shaft or growth cone. Neurite branching was determined by counting the number of neurite tips per cell. Neurite length was calculated by manually tracing the path of the longest neurite in each cell. Statistical significance was determined using an unpaired Student's t test and in this study $p < 0.05$ was considered to be statistically significant.

RESULTS

PIPP Hydrolyzes PtdIns(3,4,5)P_3

The rat homolog of PIPP hydrolyzes the phosphoinositide PtdIns(4,5)P_2 forming PtdIns(4)P in vitro (Mochizuki and Takenawa, 1999), but its ability to hydrolyze PtdIns(3,4,5)P_3 or PtdIns(3,5)P_2 has not been reported. Full-length PIPP (Figure 1A) was cloned in frame with an N-terminal FLAG tag and transiently expressed in COS-1 cells. FLAG immunoprecipitates from FLAG-PIPP or FLAG-empty vector-expressing cells were assayed for 5-phosphatase activity using PtdIns([^{32}P]3,4,5)P_3 or PtdIns([^{32}P]3,5)P_2 as the substrate. Immunoprecipitated FLAG-PIPP, but not FLAG alone, hydrolyzed PtdIns(3,4,5)P_3, forming PtdIns(3,4)P_2 (Figure 1B). However, PIPP did not hydrolyze the phosphoinositide PtdIns(3,5)P_2 (unpublished data). Immunoblot analysis demonstrated that immunoprecipitated FLAG-PIPP was expressed intact with only minor proteolysis, migrating at a higher molecular weight upon reduced SDS-PAGE (~120–130 kDa), than that predicted from the amino acid sequence as previously reported (Mochizuki and Takenawa, 1999). To evaluate whether PIPP hydrolyzes PtdIns(3,4,5)P_3 in intact cells, we utilized the pleckstrin homology (PH) domain of ARNO fused to green fluorescent protein (GFP-PH/ARNO), which binds to PtdIns(3,4,5)P_3 with high affinity and specificity and has been used as an in vivo biosensor to detect plasma membrane PtdIns(3,4,5)P_3 (Oatey *et al.*, 1999; Balla *et al.*, 2000; Dyson *et al.*, 2001). The percentage of cells overexpressing HA-PIPP versus HA-vector that demonstrated GFP-PH/ARNO recruitment to the plasma membrane in response to EGF was evaluated. Under serum-starved conditions, GFP-PH/ARNO did not localize to the plasma membrane in cells expressing either HA alone, or HA-PIPP. After 1- and 5-min EGF stimulation, GFP-PH/ARNO was detected at the plasma membrane of 62 and 70% of cells expressing empty vector, compared with 33 and 30% of cells overexpressing HA-PIPP, respectively, indicating decreased plasma membrane PtdIns(3,4,5)P_3 after ectopic PIPP expression (Figure 1C). The in vivo substrate specificity of PIPP was further investigated by determining the effect of PIPP overexpression on plasma membrane PtdIns(3,4,5)P_3, PtdIns(3,4)P_2, and PtdIns(4,5)P_2 levels in individual cells using GFP-PH/ARNO, GFP-PH/TAPP1, and PH/PLCδ1-GFP, respectively. In this assay the intensity of plasma membrane fluorescence for each phosphoinositide-biosensor was determined, relative to the intensity in the cytosol of the same cell. After growth factor stimulation, the intensity of GFP-PH/ARNO plasma membrane fluorescence relative to that detected in the cytosol increased greater than twofold in empty vector, but not PIPP-transfected cells (Figure 1D). We determined whether there was a corresponding increase in plasma membrane PtdIns(3,4)P_2 levels as a consequence of PIPP hydrolysis of PtdIns(3,4,5)P_3, by analyzing the recruitment of GFP-PH/TAPP1 to the plasma membrane. After EGF stimulation (1 min) a significant increase in GFP-PH/TAPP1 plasma membrane fluorescence was noted in both empty vector and PIPP-overexpressing cells compared with serum-starved cells. No significant difference in the recruitment of GFP-PH/TAPP1 to the plasma membrane was noted in empty vector compared with HA-PIPP-overexpressing cells at all time points. This may be a consequence of the rapid hydrolysis of PtdIns(3,4)P_2 by inositol polyphosphate 4-phosphatases, as recently described, which results in the loss of GFP-PH/TAPP1 plasma membrane localization (Ivetac *et al.*, 2005). Notably little change in the levels of plasma membrane PtdIns(4,5)P_2 were observed in PIPP-overexpressing cells compared with empty vector, as demonstrated by the fluorescence intensity of PH/PLCδ1-GFP at the plasma membrane relative to the cytosol. In control studies HA-PIPP localized to the plasma membrane in both serum-starved (unpublished data) and serum-stimulated cells, colocalizing with submembraneous actin as shown by phalloidin staining. HA-PIPP was expressed intact with minimal proteolysis (Figure 1E). Collectively these studies demonstrate PIPP rapidly hydrolyzes PtdIns(3,4,5)P_3 at the plasma membrane after growth factor stimulation.

Overexpression of PIPP Regulates Akt Phosphorylation.

The serine/threonine protein kinase Akt is a major downstream effector of PI3-kinase signaling. The PH domain of Akt binds both PtdIns(3,4,5)P_3 and PtdIns(3,4)P_2 (Franke *et al.*, 1997). Studies in SHIP1-deficient mice have revealed that both PtdIns(3,4)P_2 and PtdIns(3,4,5)P_3 are required for full Akt activation (Scheid *et al.*, 2002). Overexpression of the mammalian 5-phosphatases that hydrolyze PtdIns(3,4,5)P_3, including SHIP1, SHIP2, the type IV 5-phosphatase (also called the 72 kDa 5-phosphatase/pharbin) and SKIP in various cell lines results in decreased Ser473-Akt phosphorylation (Freeburn *et al.*, 2002; Kisseleva *et al.*, 2002; Ijuin and Takenawa, 2003; Murakami *et al.*, 2004; Sasaoka *et al.*, 2004). We evaluated the effect of ectopic PIPP expression on Ser473-Akt phosphorylation, as a marker of PI3-kinase activation. To this end, COS-1 cells transiently expressing HA-vector, or HA-PIPP, were stimulated with EGF and lysates were immunoblotted with Akt phosphorylation site-specific antibodies (phospho-Ser473-Akt), or actin antibodies (Figure 2A). The expression of wild-type PIPP reduced Ser473-Akt phosphorylation to 42 and 38% of that of HA-vector-expressing cells at 5 and 10 min, respectively (Figure 2B). EGF-stimulated cells were also analyzed for activation of the MAP/MEK kinase pathway by determining the phosphorylation status of p44/42 (Erk1/2), using phospho-specific immunoblot analysis; however, no change in phosphorylation of these proteins was noted after ectopic overexpression of PIPP (unpublished data).

PIPP Is Expressed in PC12 Cells

PIPP is the least characterized of the mammalian 5-phosphatases. Northern blot analysis has revealed that PIPP is most highly expressed in brain, heart, kidney, and stomach (Mochizuki and Takenawa, 1999). We characterized the functional role of PIPP in the rat pheochromocytoma PC12 neuronal cell line. NGF stimulates PC12 cell neurite outgrowth and elongation (Greene and Tischler, 1976) via activation of PI3-kinase signaling (Jackson *et al.*, 1996). PIPP-specific polyclonal antibodies were raised to unique PIPP peptide sequences (Figure 1A) and immune serum was affinity-purified on a peptide-coupled thiopropyl Sepharose column. Affinity-purified PIPP antibodies immunoblotted a single

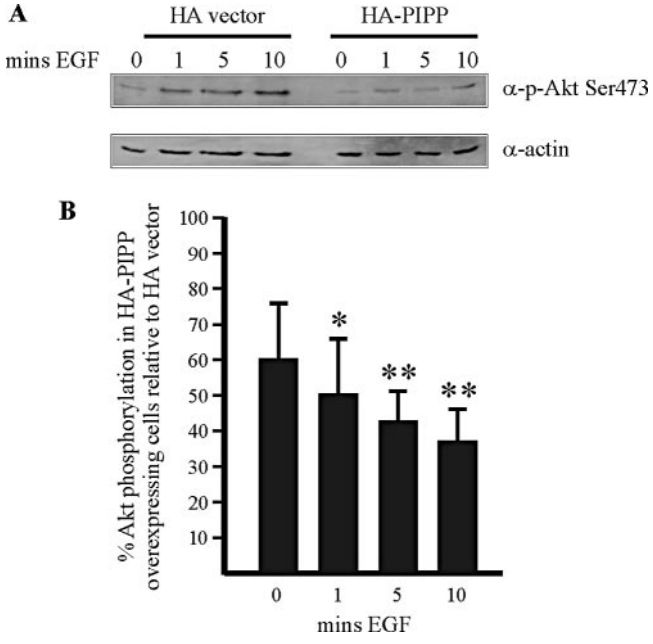

Figure 2. PIPP expression inhibits Ser473-Akt phosphorylation. (A) COS-1 cells were transiently transfected with plasmids encoding either HA-vector or HA-PIPP. Serum-starved cells were stimulated with 100 ng/ml EGF for 0–10 min and 50 μg of cell lysates was immunoblotted with antibodies specific for phospho-Ser473-Akt, or actin (loading control) or HA (unpublished data). (B) The relative level of phospho-Ser473-Akt was determined by densitometry, standardized to actin loading control, and expressed as a percentage of that detected in HA-vector cell lysates, from three independent experiments. (* $p < 0.05$, ** $p < 0.01$).

polypeptide species of ~120–130 kDa in lysates from serum-starved or NGF-stimulated PC12 cells, consistent with the molecular weight of recombinant PIPP (Figure 3A). The level of PIPP protein expression, relative to an actin loading control, did not change significantly during NGF-stimulated PC12 differentiation for up to 4-d stimulation.

PIPP Localizes to the Neurite Shaft and Growth Cone of Differentiated Neurites

After NGF stimulation, PC12 cells cease proliferating and undergo neuronal differentiation (Halegoua *et al.*, 1991). Within hours of NGF stimulation, small actin-rich neurites bud from the plasma membrane and one or more may subsequently extend over several days, forming differentiated neurites that are longer in length than the diameter of the cell body (Paves *et al.*, 1988; Aoki *et al.*, 2004). Ectopic expression of recombinant tagged PIPP in COS-1 cells results in its constitutive association with the plasma membrane, under both serum-starved and EGF-stimulated conditions, mediated by its C-terminal SKICH domain (Mochizuki and Takenawa, 1999; Gurung *et al.*, 2003). However, the localization of endogenous PIPP has not been reported. After 3-d NGF stimulation both differentiated PC12 cells bearing long neurites (~20–30% of cells) and undifferentiated cells were detected as shown by phalloidin staining of actin. Indirect immunofluorescence using affinity-purified PIPP antibodies demonstrated staining at the plasma membrane and cytosol of undifferentiated cells, and in differentiated cells, PIPP localized to the cytosol and plasma membrane of the cell body and prominently at the growth cone of differentiated neurites (Figure 3B; see arrows for growth cones). Preimmune staining was nonreactive, as was PIPP immune serum, which was preabsorbed against the immunogenic PIPP peptide. Higher power images revealed, after 4-h NGF stimulation, short actin-rich neurite buds detected by Texas Red-conjugated phalloidin revealing neurite initiation, but despite faint PIPP staining at some neurite projections, PIPP did not colocalize with the majority of actin-rich spikes, and staining was most intense at the plasma membrane (Figure 3C, top row, arrowheads show actin-rich neurite spikes). After neurite initiation, PIPP staining was prominent at the distal end of the developing neurite (Figure 3C, second row; see arrow). PIPP showed only partial colocalization with actin in these developing neurites. After 3-d NGF stimulation, cytosolic PIPP staining was detected at the cell body, and in some cells nuclear staining was evident. By this stage PIPP staining showed increased intensity at the distal neurite shaft, appearing most concentrated at the growth cone (Figure 3C, third row, arrow indicates growth cone). In higher power images analysis of the intensity of PIPP staining along the neurite shaft demonstrated little at the neurite shaft close to the cell body, but increased intensity along the shaft, with the highest levels at the growth cone (Figure 3D). We also ectopically overexpressed HA-PIPP in differentiated PC12 cells that had been stimulated with NGF for 2 d before transfection. Indirect immunofluorescence using anti-HA antibodies revealed cytosolic HA-PIPP localization in the cell body, and, in addition, HA-PIPP was detected in the neurite shaft and prominently at the growth cone (Figure 3E). Anti-HA staining of empty vector-expressing cells demonstrated cytosolic staining of the cell body only (unpublished data). Previous studies have identified a C-terminal domain designated the "SKICH" domain, which is also found in the 5-phosphatase SKIP, that contributes to the intracellular membrane localization of both SKIP and PIPP (Gurung *et al.*, 2003). HA-PIPP^{SKICH} localized in a similar distribution to the full-length recombinant protein, demonstrating prominent localization at the growth cone (Figure 3E)

In differentiating neurons, microtubules localize to the growth cone and neurite shaft, regulating neurite extension (reviewed in Lee and Van Vactor, 2003). In initiated cells, PIPP-rich neurite projections were detected in areas devoid of β-tubulin staining (Figure 3F, top row). In NGF-differentiated neurites, β-tubulin staining was evident at the cell body, neurite shaft, and growth cone, colocalizing with PIPP most prominently at the latter site (Figure 3F, middle and bottom rows; see arrows for growth cones). PIPP demonstrated patchy colocalization with microtubules along the neurite shaft and in the central domain of the growth cone. However, PIPP distribution extended further distally into the growth cone, relative to β-tubulin staining (Figure 3F, middle and bottom rows; arrows indicate PIPP growth cone staining).

Overexpression of PIPP Inhibits NGF-stimulated Neurite Elongation

PI3-kinase signaling plays a critical role in neuronal cell differentiation. Loss of PI3-kinase activity inhibits the differentiation of PC12 cells (Kimura *et al.*, 1994; Jackson *et al.*, 1996; Kim *et al.*, 2004). Because PIPP hydrolyzes PtdIns(3,4,5)P_3 and regulates Akt phosphorylation, we reasoned that the overexpression of PIPP, but not catalytically inactive PIPP, may modulate specific PI3-kinase-dependent events that govern PC12 cell differentiation. After 24-h NGF stimulation, cells overexpressing HA-PIPP, mutant inactive PIPP (HA-PIPP^{H557A}) that contains a single point mutation in a critical catalytic amino acid, histidine 557 (Whisstock *et*

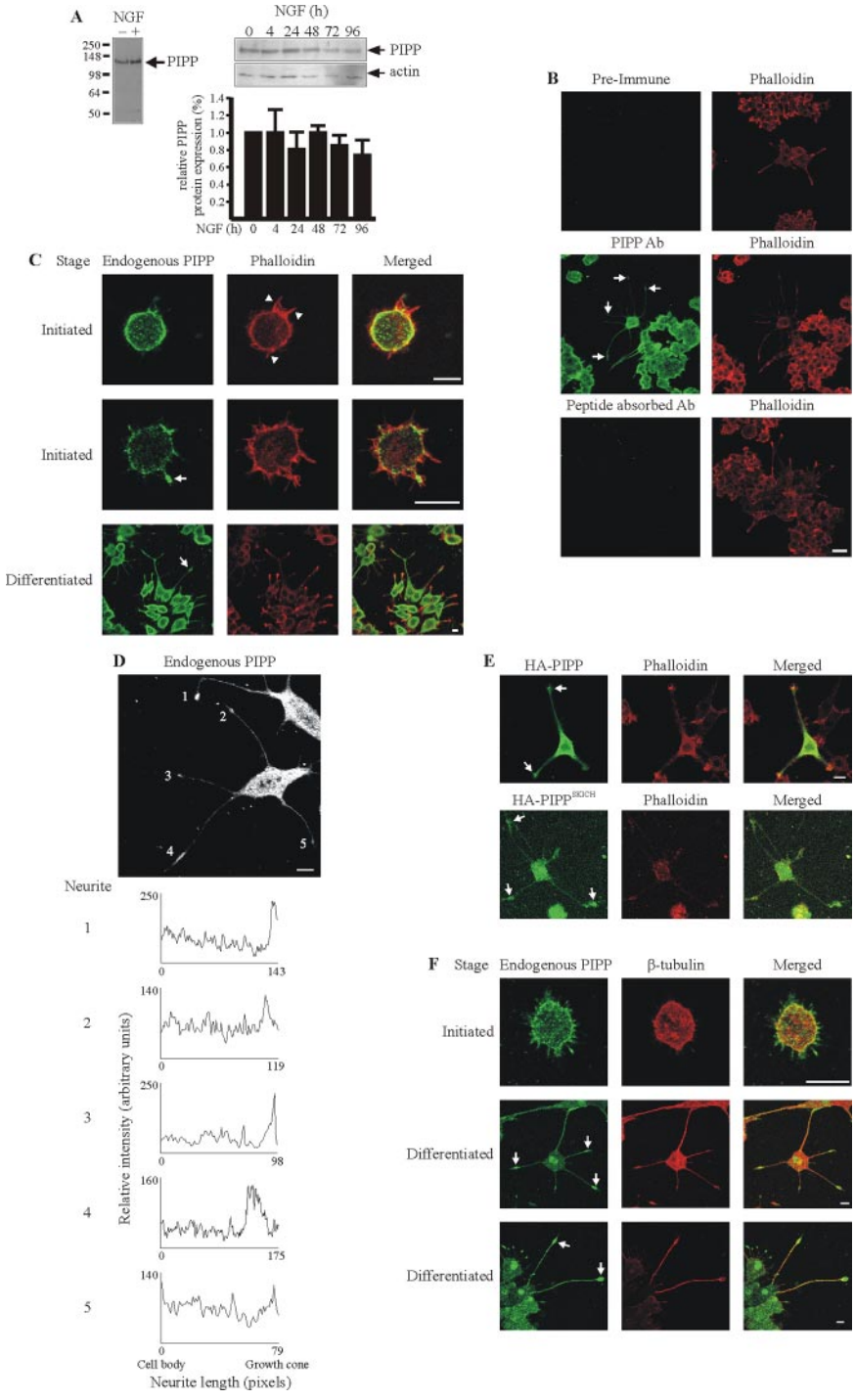

Figure 3. PIPP localization in undifferentiated and NGF differentiated PC12 cells. (A) PC12 cells were either left unstimulated (−) or stimulated with 100 ng/ml NGF for 16 h (+). Cell lysates (20 μg) were immunoblotted with affinity-purified PIPP antibodies. Molecular weight markers are indicated on the left and immunoreactive endogenous PIPP is indicated by the arrow. PC12 cells were stimulated with 100 ng/ml NGF for 0–96 h. Cell lysates (20 μg) were immunoblotted with PIPP affinity-purified antibodies. The membrane was reprobed with actin antibodies as a loading control. The average expression of PIPP was determined by densitometric quantification of PIPP immunoreactive peptides, relative to actin from two separate experiments, with expression at day 0 arbitrarily scored as 1. (B) PC12 cells were grown on 0.01% poly-L-lysine-coated coverslips overnight and then stimulated to differentiate with 100 ng/ml NGF for 3 d. Cells were fixed and permeabilized then stained with preimmune serum (pre-immune), PIPP-specific antibodies (PIPP Ab), or PIPP-immune serum that had been preabsorbed with free peptide (Peptide absorbed Ab). Cells were costained with Texas Red phalloidin and visualized by confocal microscopy. Arrows show growth cone staining. Scale bar, 10 μm. (C) PC12 cells were grown on 0.01% poly-L-lysine-coated coverslips overnight and stimulated to differentiate with 100 ng/ml NGF for 4–72 h. Fixed cells were stained with affinity-purified PIPP antibodies and costained with either Texas Red phalloidin (C) or β-tubulin antibodies (F). Merged images are shown on the right. Arrow head indicates actin-rich neurite spikes, devoid of PIPP staining. Arrow indicates PIPP staining at the growth cone. (D) Fluorescence intensity after anti-PIPP immunostaining of representative neurite shafts after 72-h NGF stimulation. Neurite length at 0 represents fluorescence intensity immediately adjacent to the cell body. Scale bar, 10 μm. (E) PC12 cells were stimulated to differentiate with 100 ng/ml NGF for 2 d and then transiently transfected with HA-PIPP or HA-PIPP^{SKICH}. Cells were treated with 100 ng/ml NGF for a further 24 h, then fixed and costained with HA antibodies and Texas Red phalloidin. Arrows indicate growth cone staining. Scale bars, 10 μm

al., 2000), or HA-vector, were scored for neurite initiation, defined as thin actin-rich extensions less than one cell body diameter in length. No difference in neurite initiation was apparent in PIPP versus empty vector-overexpressing neurites (unpublished data). After 3-d NGF stimulation, cells were classified as differentiated upon the acquisition of one or more neurites that were greater in length than the diameter of the cell body. By day 3, between ~30–40% of empty vector, but only ~10% of PIPP-overexpressing cells demonstrated differentiated neurites (unpublished data). Many PIPP-overexpressing cells demonstrated actin-rich projections but did not exhibit elongated neurites. For example, most HA-PIPP-overexpressing PC12 cells bore short neurites, whereas adjacent untransfected cells exhibited neurites greater in length than the cell body diameter (Figure 4A; see arrow for HA-PIPP-expressing cell and star for adjacent untransfected cell). The number of PIPP-expressing PC12 cells exhibiting differentiated neurites was expressed as a ratio of that detected in empty-vector cells. No significant difference was detected after 1-d NGF stimulation; however, after 2 and 3 d, PIPP-expressing cells showed a 65 ± 9.8 and 70 ± 6.4% respective reduction in the number of cells bear-

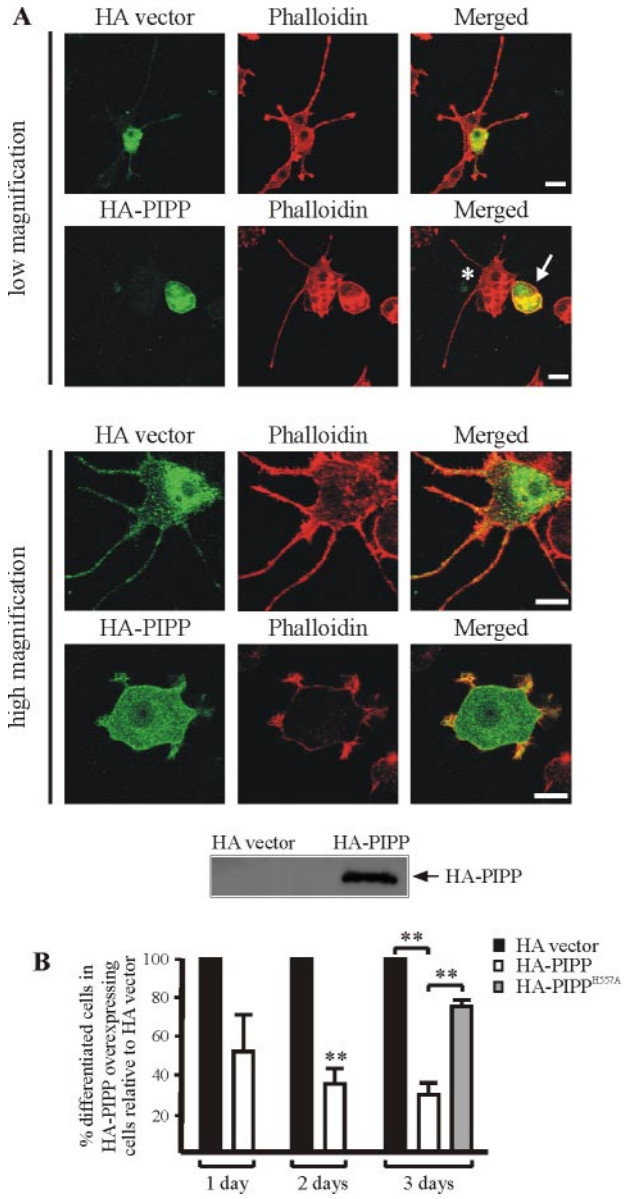

Figure 4. Overexpression of PIPP impairs neurite elongation in NGF-treated PC12 cells. (A) PC12 cells were transiently transfected with plasmids encoding either HA alone or HA-PIPP and stimulated with 100 ng/ml NGF for 3 d. Fixed cells were costained with HA antibodies and Texas Red phalloidin, and representative images are shown (* untransfected cell; arrow indicates HA-PIPP transfected cell). Scale bar, 20 μm in low- and 10 μm in high-magnification images. Merged images are shown on the right. Cell lysates (20 μg) from PC12 cells transfected with HA-vector or HA-PIPP were immunoblotted with an HA antibody. PIPP migration is indicated by the arrow. (B) HA-vector, wild-type HA-PIPP, or catalytically inactive PIPP (HA-PIPP^{H557A})-transfected cells were NGF-stimulated for 3 d, fixed, and stained with HA antibodies. The number of cells exhibiting neurites greater in length than the diameter of the cell body was calculated for HA-PIPP- (open bars) and HA-PIPP^{H557A}- (gray bars) expressing cells and expressed as a percentage of that detected in HA-vector (black bars)-transfected PC12 cells. Bars represent the mean ± SEM of 150 cells scored for each construct in each of three separate transfections. (** $p < 0.01$).

ing differentiated neurites, relative to empty vector-expressing cells. In contrast, cells overexpressing HA-PIPP^{H557A} exhibited a significantly increased number of differentiated neurites relative to wild-type PIPP overexpression, similar to empty vector-expressing cells (Figure 4B), suggesting PIPP catalytic activity is critical for PIPP-dependent inhibition of neurite differentiation. To characterize the intensity and distribution of polymerized actin and microtubules, PC12 cells were stained with Texas Red phalloidin (Figure 4A) or β-tubulin antibody (unpublished data). The majority of PIPP-overexpressing cells did not develop neurites greater in length than the diameter of the cell body and as a consequence phalloidin and β-tubulin staining of the short neurites could not be used to assess neurite shaft or growth cone distribution of actin or microtubules (unpublished data). Therefore, PIPP appears not to regulate neurite initiation, but may negatively modulate specific stages of neurite differentiation.

Targeted Depletion of PIPP Promotes Neurite Hyperelongation

To assess the contribution of PIPP to NGF-stimulated neurite differentiation, we utilized targeted depletion of PIPP using RNA interference (RNAi; Figure 5A). Stable cell lines underexpressing PIPP were generated by cloning oligonucleotides designed to unique PIPP sequences (PIPP RNAi), or the same sequence scrambled (scrambled RNAi), into the psiRNA-hH1 vector followed by stable transfection into PC12 cells. Individual clones underexpressing PIPP or the scrambled controls were selected and grown in the presence of G418. PIPP immunoblot analysis demonstrated a ~60–65% reduction in PIPP protein levels in PIPP RNAi clones (1, 5, and 8), relative to scrambled RNAi clones (4 and 5), standardized to Akt or β-tubulin as loading controls (Figure 5B). Two PIPP RNAi clones (1 and 8) were used for all subsequent studies and compared with the corresponding scrambled RNAi clones (4 and 5).

Several studies have indicated a role for PI3-kinase in NGF-stimulated neurite initiation. For example, wortmannin treatment inhibits early NGF-stimulated morphological responses including actin-rich microspike formation and neurite outgrowth (Jackson *et al.*, 1996). Overexpression of constitutively active PI3-kinase results in spontaneous neurite outgrowth in the absence of NGF treatment (Kobayashi *et al.*, 1997). We investigated whether PIPP RNAi-mediated depletion results in spontaneous neurite outgrowth, in the absence of NGF stimulation. To this end, PC12 cells were grown on coverslips for up to 5 d in serum but without NGF, fixed, and stained with Texas Red-conjugated phalloidin. Cells were examined for evidence of neurite initiation, including actin-rich spikes and/or neurite projections. No significant difference in neurite initiation was detected in the absence of NGF stimulation in PIPP RNAi versus scrambled RNAi clones for up to 5 d (unpublished data), indicating that PIPP targeted depletion is not sufficient to promote spontaneous neurite initiation.

After 3-d NGF stimulation, both scrambled RNAi and PIPP RNAi cells demonstrated extensive neurite outgrowth with many neurites greater in length than the diameter of the cell body, similar to untransfected cells. Although a significantly greater number of cells were differentiated by 5-d NGF stimulation in all RNAi clones, to adequately image and assess the PIPP-dependent phenotype (see below), analysis was performed after only 3-d NGF stimulation. The number of cells bearing differentiated neurites greater in length than the diameter of the cell body in all PIPP RNAi clones after 3-d NGF differentiation was expressed as a percentage of that detected in all scrambled RNAi clones, revealing a >1.7-fold increase upon targeted depletion of

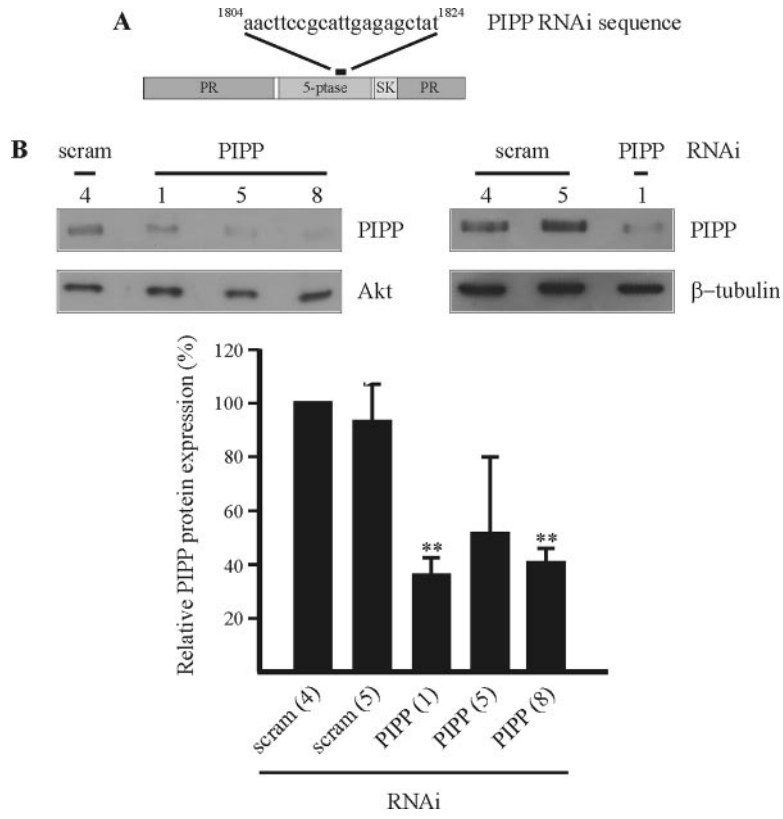

Figure 5. Targeted depletion of PIPP by RNAi. (A) The unique PIPP sequence used to generate PIPP RNAi clones is indicated. (B) Cells stably transfected with the PIPP RNAi sequence or a scrambled RNAi control were harvested and 20 μg protein was separated by SDS-PAGE and immunoblotted with PIPP or Akt protein or β-tubulin antibodies as a protein loading control. The relative PIPP protein expression in PIPP RNAi clones 1, 5, and 8 was determined by densitometry of immunoreactive polypeptides, standardized to Akt or β-tubulin loading control and expressed as a percentage of that detected in RNAi-scrambled clone 4, which was designated 100%. Results represent the mean $\pm$ SEM of nine independent experiments. (**$p < 0.01$).

PIPP (Figure 6A). In addition, we noted that PIPP RNAi differentiated PC12 cells exhibited neurites that were significantly longer than scrambled RNAi neurites (Figure 6B). Thirty percent of PIPP RNAi versus 10% of scrambled RNAi PC12 cells exhibited neurites that were longer than four diameters of the cell body (Figure 6C). Because siRNAs can exert nonspecific effects, we investigated whether cotransfection of HA-PIPP cDNA could suppress the knock-down phenotype of PIPP RNAi PC12 cells. To this end, PIPP RNAi clones were transfected with 5 μg of wild-type HA-PIPP or HA-empty vector cDNA and neurites assessed following 3-d NGF treatment. On overexpression of wild-type HA-PIPP cDNA, PIPP RNAi neurites resembled scrambled RNAi neurites (unpublished data). A significant reduction in the percentage of cells bearing long neurites correlated with transfection of wild-type HA-PIPP cDNA, but not empty vector cDNA, into PIPP RNAi clones. (Figure 6D). To further evaluate the PIPP-RNAi hyperelongated phenotype, the average neurite length was determined after 3-d NGF stimulation. Scrambled RNAi neurites exhibited average lengths of 31.7 $\pm$ 2.5 and 32.0 $\pm$ 2.4 μm (clones 4 and 5, respectively), whereas PIPP RNAi neurites showed a 1.6-fold increase in average length at 48.1 $\pm$ 1.5 and 52.5 $\pm$ 3.9 μm (clones 1 and 8, respectively; Figure 6E).

We also investigated whether PIPP underexpression altered neurite branching, because previous studies suggested that expression of constitutively active PI3-kinase or Akt, or global inhibition of GSK-3β using a specific inhibitor promotes axonal branching (Hall *et al.*, 2002; Higuchi *et al.*, 2003; Jones *et al.*, 2003). The number of branching neurites was determined in NGF-stimulated PIPP RNAi cells and compared with scrambled RNAi controls, but no difference was detected (Figure 6F). It is possible that PIPP growth cone localization in differentiating neurites may preclude its access to PtdIns(3,4,5)P_3-dependent signaling events at the cell body or neurite shaft that act to promote neurite branching.

To establish whether PIPP underexpression promotes neurite hyperelongation as a consequence of enhanced PI3-kinase signaling, cells were treated with the PI3-kinase inhibitors wortmannin or LY294002. Inhibition of PI3-kinase-dependent neurite differentiation requires the frequent addition of wortmannin over 3 d, because this inhibitor is unstable in tissue culture within 5 h of its addition (Kimura *et al.*, 1994; Jackson *et al.*, 1996). Other studies using less intense wortmannin regimes have shown that inhibition of neurite elongation can be achieved after treatment with wortmannin, commenced up to 25 h after NGF stimulation with repeated doses provided every 5 h (Kimura *et al.*, 1994). Because we aimed to specifically determine the interdependency between the PIPP-dependent neurite hyperelongated phenotype and PI3-kinase signaling, rather than the well-characterized PI3-kinase-dependent neurite differentiation and elongation events, we treated NGF-differentiating cells with a low-dose wortmannin treatment (100 nM) daily for 3 d or with LY294002 (50 μM), which is a more stable PI3-kinase inhibitor, on the indicated days. After treatment with either inhibitor the percentage of differentiated neurites in scrambled or PIPP RNAi clones did not decrease (unpublished data); however, wortmannin or LY294002 significantly inhibited the hyperelongated phenotype exhibited by PIPP RNAi neurites. For example, the percentage of cells showing hyperelongated neurites (cells bearing neurites greater in length than four times the diameter of the cell body) in PIPP RNAi clones decreased from 29 to 12% upon wortmannin treatment, reaching levels similar to those detected in untreated scrambled RNAi cells (Figure 6G). As anticipated no significant difference was noted when wortmannin or LY294002 was added before versus 24 h after the

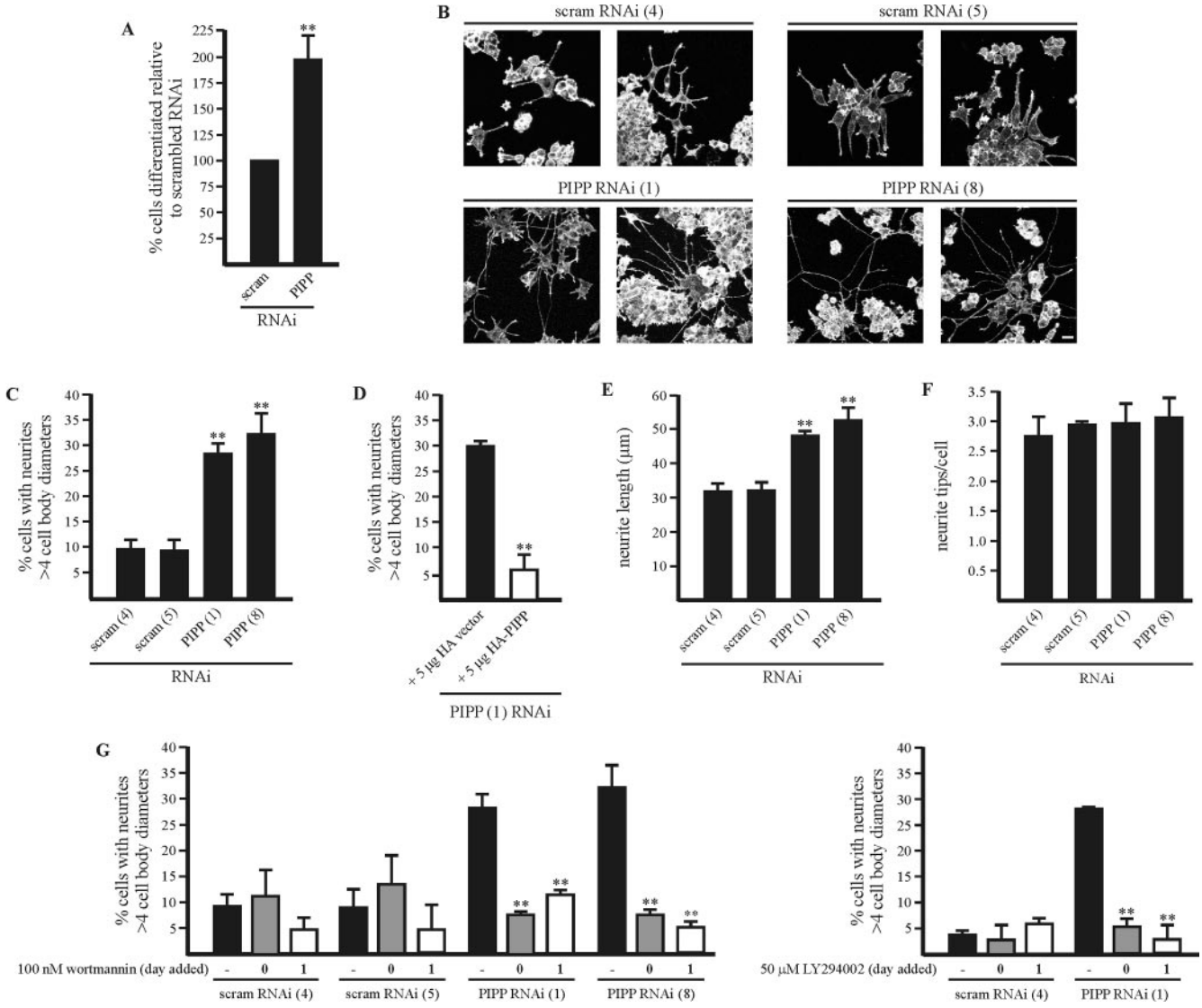

Figure 6. Targeted depletion of PIPP results in hyperelongated neurites. (A) Cells stably transfected with PIPP RNAi or a scrambled RNAi control were grown overnight on coverslips and then treated with 100 ng/ml NGF for 3 d. Cells were fixed and stained with Texas Red phalloidin to image differentiated neurites. Cells were scored as differentiated upon the acquisition of neurites greater in length than the diameter of the cell body. Results represent the mean ± SEM of three independent differentiation experiments in which 160 cells were scored for each RNAi clone (two scrambled and two PIPP RNAi). Results are expressed as a percentage of that detected in scrambled RNAi clones, which were designated 100%. (**$p < 0.01$). (B) Representative images of scrambled (4 and 5) RNAi clones (top panel) and PIPP RNAi clones (1 and 8) that were NGF-differentiated for 3 d, stained with Texas Red phalloidin, and imaged using confocal microscopy. Scale bar, 20 μm. (C) The percentage of cells bearing hyperelongated neurites (defined as neurite length greater than four cell body diameters) was determined for each indicated RNAi clone. Results represent the mean ± SEM (** $p < 0.01$) of at least 16 cells scored for each RNAi clone for seven separate differentiation experiments (>100 neurites scored per RNAi clone). (D) PIPP RNAi clone (1) cells were transiently transfected with plasmids encoding either HA-alone (black bar) or HA-PIPP (open bar). Cells were differentiated with 100 ng/ml NGF for 3 d, and the percentage of cells bearing hyperelongated neurites (>4 cell body diameters) was determined. Results represent the mean ± SEM of at least 10 cells scored for each construct for three separate transfections (>59 cells scored per construct; ** $p < 0.01$). (E) Scrambled and PIPP RNAi clones were differentiated with 100 ng/ml NGF for 3 d. Neurites were manually traced using Image J software to measure length. Bars represent the mean ± SEM of at least 15 neurites measured for each of the indicated RNAi clones in six separate differentiation experiments (>90 neurites per RNAi clone; ** $p < 0.01$). (F) Neurites were scored for the number of branches. Results represent the mean ± SEM of three separate experiments in which >50 neurites for each RNAi clone were scored for the presence of neurite branching. (G) Scrambled or PIPP RNAi clones were either untreated (black bars) or treated daily with wortmannin (100 nM) or once with LY294002 (50 μM), either commencing immediately before NGF stimulation (0; gray bars) or 24 h after the commencement of NGF stimulation (1; open bars). The percentage of cells bearing hyperelongated neurites (defined as neurite length greater than four cell body diameters) was determined for each clone. Results are the mean ± SEM for at least 17 cells scored for the indicated RNAi clones for 2–3 separate differentiation experiments (total >38 cells scored per RNAi clone; ** $p < 0.01$).

commencement of NGF stimulation. In scrambled RNAi clones, very few neurites were greater in length than four times the diameter of the cell body (~10%), so wortmannin or LY294002 treatment at these doses had no significant

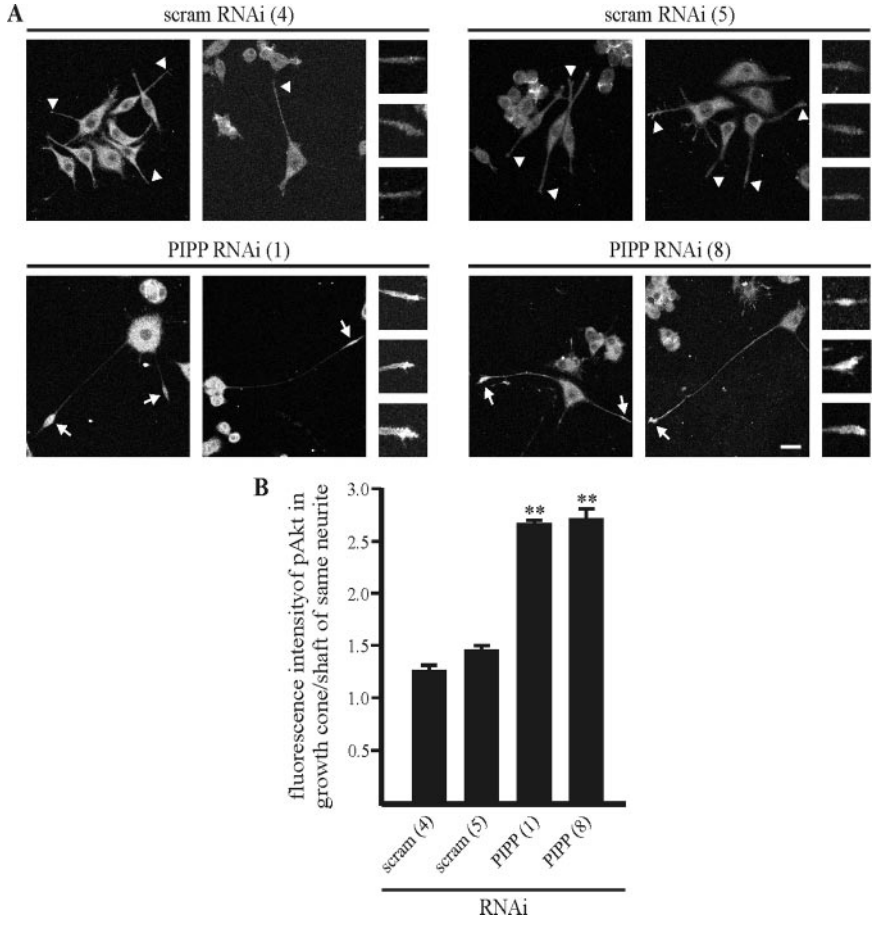

Figure 7. PIPP regulates the spatial distribution of phospho-Ser473-Akt at the growth cone. (A) RNAi clones were NGF-differentiated for 3 d, fixed and stained with phospho-Ser473-Akt antibodies (immunohistochemistry-specific), and imaged at the same laser attenuation. Phospho-Ser473-Akt fluorescence at the growth cone of PIPP RNAi clones is indicated by arrows, whereas the growth cone staining in scrambled RNAi clones is shown by arrowheads. In addition, in the small panels on the right-hand side, additional growth cones are shown at the same laser attenuation and at higher magnification for each indicated clone. Scale bar, 20 μm. (B) The fluorescence intensity of phospho-Ser473-Akt staining at the growth cone, as a ratio of that detected at the shaft of the same neurite, was determined using Image J software measuring the average pixel intensity within a box of defined size (5 $\times$ 15 pixels for growth cone and 5 $\times$ 25 pixels for neurite shaft). Bars represent the mean $\pm$ SEM of neurites scored per indicated clone for two separate differentiation experiments (>25 neurites scored for each RNAi clone indicated; ** $p < 0.01$).

effect. Therefore, PIPP RNAi-induced neurite hyperelongation is exquisitely sensitive to PI3-kinase inhibition, suggesting that loss of PIPP 5-phosphatase activity enhances PI3-kinase signaling, which in turn leads to neurite hyperelongation.

NGF-stimulated axon growth is mediated by PI3-kinase-dependent Akt and/or ILK activation, which lead to GSK-3β phosphorylation at Ser9 inactivating the kinase (Mills *et al.*, 2003; Zhou *et al.*, 2004; Jiang *et al.*, 2005). This in turn facilitates dephosphorylated adenomatous polyposis coli (APC) protein binding to microtubule plus ends, promoting microtubule assembly (Zumbrunn *et al.*, 2001; Zhou *et al.*, 2004). To investigate whether targeted depletion of PIPP results in enhanced Akt activation, cell lysates derived from NGF-differentiated scrambled versus PIPP RNAi clones were immunoblotted using specific phospho-Ser473-Akt antibodies and standardized for protein loading using total Akt protein antibodies. No significant difference in the ratio of phospho-Ser473-Akt/total Akt was noted between NGF-differentiated scrambled versus PIPP RNAi PC12 cells (unpublished data). We have demonstrated here that PIPP is most concentrated at the growth cone of differentiated PC12 neurites. It has been previously reported that in neurons, phospho-Ser473-Akt localizes to both the cell body and the leading edge of the growth cone, with little detected at the neurite shaft (Zhou *et al.*, 2004). Therefore, PIPP may regulate the spatial distribution of phospho-Ser473-Akt specifically at the growth cone, rather than regulating the total cellular complement of phospho-Ser473-Akt. To investigate this contention, NGF-stimulated RNAi clones were stained with an immunohistochemistry-specific phospho-Ser473-Akt antibody and examined by indirect immunofluorescence. Others have reported that specific fixation techniques are required to image phospho-Ser473-Akt in neurons, which we utilized here in PC12 cells (Zhou *et al.*, 2004). Enhanced phospho-Ser473-Akt staining was noted at the growth cone of differentiated PIPP RNAi, compared with scrambled RNAi PC12 cells, when cells were prepared under the same conditions and imaged at the same laser attenuation (Figure 7A; see arrows). To evaluate the spatial distribution of phospho-Ser473-Akt, the intensity of phospho-Ser473-Akt staining at the growth cone, relative to the shaft of the same neurite was determined. An approximately twofold increase in the intensity of phospho-Ser473-Akt fluorescence in the growth cone of PIPP RNAi clones 1 and 8, relative to the shaft of the same neurite, was demonstrated above that detected in the corresponding scrambled RNAi neurites (Figure 7B). A similar analysis of the spatial distribution of total Akt protein staining at the growth cone, relative to the same neurite shaft, showed no significant difference in PIPP RNAi versus scrambled RNAi cells (unpublished data). Therefore, PIPP may regulate the spatial distribution of phospho-Ser473-Akt in differentiating neurites, specifically at the growth cone.

To determine whether PtdIns(3,4,5)P_3 accumulates at the growth cone in PIPP RNAi neurites, cells were transfected with the construct GFP-PH/ARNO. Transfection of this construct before NGF treatment blocks neurite differentiation presumably by sequestering PtdIns(3,4,5)P_3 (unpublished data); therefore cells were transfected with this construct after 2-d NGF stimulation and observed 24 h after transfec-

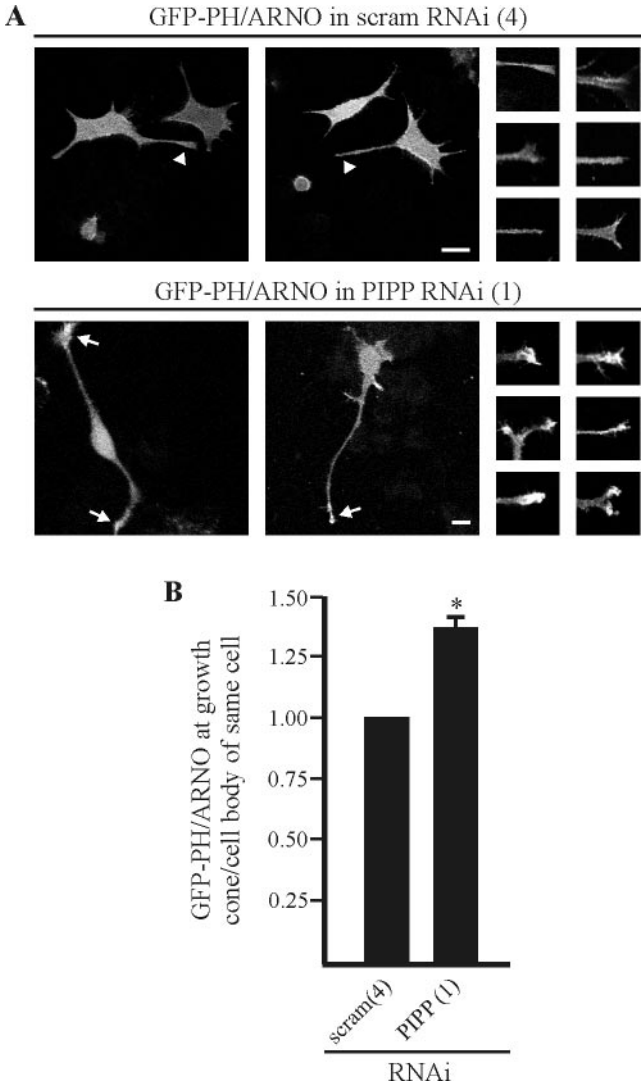

Figure 8. PIPP regulates the spatial distribution of PtdIns(3,4,5)P_3 at the growth cone. (A) Scrambled or PIPP RNAi clones were differentiated with 100 ng/ml NGF for 48 h and then transiently transfected with GFP-PH/ARNO. Cells were differentiated with NGF for a further 24 h before being fixed and imaged at the same laser attenuation. Examples of differentiated neurites from scrambled RNAi clone 4 and PIPP RNA clone 1 are demonstrated and in addition in the small panels on the right-hand side, additional growth cones are shown at the same laser attenuation and at higher magnification for each indicated clone. Scale bar, 20 μm. (B) The relative fluorescence intensity of GFP-PH/ARNO accumulation at the growth cone, as a ratio of the average GFP fluorescence in the cell cytosol was determined for each RNAi clone using Image J software. At the growth cone the average fluorescence intensity of the brightest region was measured, and for cell cytosol measurements, the average fluorescence intensity over three discrete areas was determined. Bars represent the mean ± SEM of growth cones scored per indicated clone for two separate differentiation experiments (>25 neurites scored for each RNAi clone; $p^* < 0.05$).

tion. It was noteworthy that GFP-PH/ARNO localization was more prominent at the growth cone of PIPP RNAi clones than scrambled controls (Figure 8). To assess the accumulation of PtdIns(3,4,5)P_3 at the growth cone and to standardize for different levels of expression of the fusion protein, all cells were examined at the same laser attenuation and the intensity of fluorescence at the growth cone was determined relative to the cytosol of the same cell body (Figure 8). Notably PIPP RNAi neurites demonstrated enhanced (~1.4-fold) GFP-PH/ARNO accumulation at the growth cone, relative to the cell body cytosol compared with scrambled RNAi cells, consistent with the contention that PtdIns(3,4,5)P_3 accumulates at the growth cone as a consequence of PIPP knock-down.

GSK-3β is a signaling mediator that acts downstream of PI3-kinase to promote neurite extension via regulation of microtubule assembly (Zhou *et al.*, 2004). Phosphorylated Ser9-GSK-3β is concentrated at the cell body and distal end of the axon growth cone in differentiated hippocampal neurons (Jiang *et al.*, 2005). It has been proposed that the spatial inactivation of GSK-3β by the PI3-kinase signaling pathway occurs at the growth cone, which in turn promotes axonal elongation (Zhou *et al.*, 2004). We determined whether PIPP could regulate the total cellular levels of phospho-Ser9-GSK-3β or the localized inactivation of this kinase. Immunoblot analysis of lysates from NGF-differentiated PC12 cells revealed no difference in the ratio of phospho-Ser9-GSK-3β/total GSK-3β levels in PIPP RNAi relative to scrambled RNAi cells (unpublished data). To determine if the spatial distribution of phospho-Ser9-GSK-3β was altered as a consequence of enhanced PI3-kinase signaling at the growth cone in PIPP-depleted cells, NGF-differentiated PC12 cells were examined by indirect immunofluorescence using phospho-Ser9-GSK-3β antibodies (Figure 9A). The intensity of this staining at the growth cone was determined relative to the intensity of total GSK-3β protein antibody staining at this site (Figure 9B). Increased intensity of phospho-Ser9-GSK-3β antibody staining at the growth cone was demonstrated in PIPP RNAi-differentiated neurites compared with scrambled RNAi neurites (Figure 9A). PIPP RNAi neurites showed an increased (~1.4-fold) ratio of phospho-Ser9-GSK-3β/total GSK-3β protein fluorescence intensity at the growth cone, relative to scrambled RNAi neurites (Figure 9B). In addition, the spatial distribution of phospho-Ser9-GSK-3β at the growth cone, relative to the shaft of the same neurite was enhanced 2.5- and 3.2-fold in PIPP RNAi clones 1 and 8, respectively, relative to scrambled RNAi controls (Figure 9C). Collectively, these studies suggest that PIPP regulates the spatial distribution of Ser9-GSK-3β phosphorylation and therefore its inactivation at the growth cone.

Neurite elongation is mediated by multiple signaling pathways and by complex interactions between actin remodeling and microtubule dynamics (Baas and Luo, 2001). Differentiated PC12 cells were fixed and stained with Texas Red phalloidin and imaged by confocal microscopy to visualize polymerized actin in the cell body, neurite shaft, and growth cone. No overt differences in the level or distribution of polymerized actin were noted in PIPP RNAi neurites or growth cones, compared with scrambled controls (Figure 6B). PI3-kinase-dependent phosphorylation of GSK-3β at Ser9 leads to its inactivation (Cross *et al.*, 1995) and therefore GSK-3β substrates including the microtubule-associated proteins MAP1B (microtubule-associated protein 1B), CRMP-2, tau, and APC are not phosphorylated by this kinase, which in turn promotes microtubule polymerization and stability (Goold *et al.*, 1999; Zumbrunn *et al.*, 2001; Cho and Johnson, 2004; Zhou *et al.*, 2004; Yoshimura *et al.*, 2005; Zhou and Snider, 2005). The polymerization of microtubules facilitates axon elongation (Zhou and Snider, 2005). Microtubule polymers in neurites were visualized by directly extracting and fixing the neurites at the same time to eliminate tubulin monomers (He *et al.*, 2002), followed by staining of polymerized microtubules with β-tubulin antibodies.

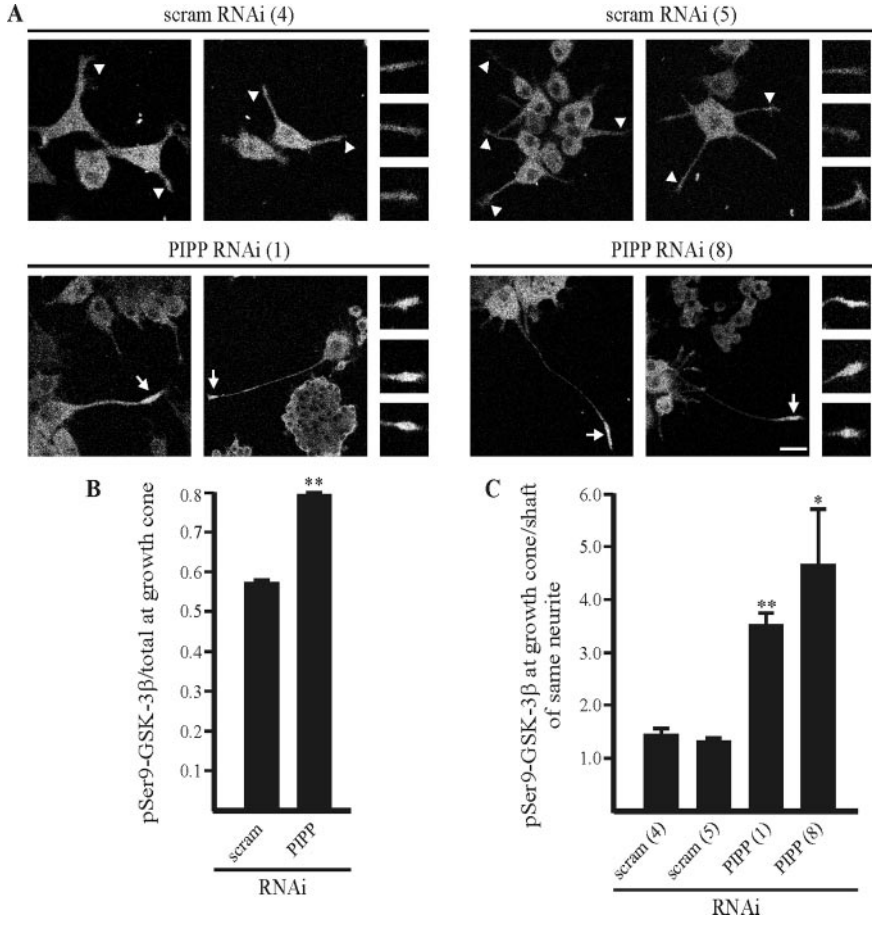

Figure 9. PIPP regulates the spatial distribution of phospho-Ser9-GSK-3β at the growth cone. (A) The indicated RNAi clones were stimulated with NGF for 3 d, fixed and stained with phospho-Ser9-GSK-3β as shown or with GSK-3β protein antibodies (unpublished data), and examined by confocal microscopy at the same laser attenuation. Phospho-Ser9-GSK-3β fluorescence at the growth cone of PIPP and scrambled RNAi clones is indicated by arrows and arrowheads, respectively. Examples of differentiated neurites from scrambled RNAi clones 4 and 5, and PIPP RNA clones 1 and 8 are shown and, in addition, in the small panels on the right-hand side, additional growth cones are shown at the same laser attenuation and at higher magnification for each indicated clone. Scale bar, 20 μm. (B) Bars represent the mean $\pm$ SEM of the fluorescence intensity of phospho-Ser9-GSK-3β as a ratio of total GSK-3β protein staining intensity at the growth cone for >25 neurites per RNAi clone. Average pixel intensity at the growth cone within a 20 $\times$ 10-pixel box was determined using Image J software (**$p < 0.01$). (C) The fluorescence intensity of phospho-Ser9-GSK-3β protein staining intensity at the growth cone as a ratio of the staining intensity at the shaft of the same neurite was determined using Image J software. The average pixel intensity was measured in a 20 $\times$ 10 pixel box at the growth cone and a 40 $\times$ 10-pixel box on the neurite shaft. Bars represent the mean $\pm$ SEM of 15 neurites scored per indicated clone for three separate differentiation experiments (>45 neurites for each RNAi clone; * $p < 0.05$, ** $p < 0.01$).

Cells were imaged using the same laser attenuation and the relative intensities of β-tubulin staining in the neurite shafts were determined. Previous studies using this technique have demonstrated a >50% decrease in the localized intensity of microtubule polymers in the hippocampal neuron shaft after PI3-kinase inhibition by LY294002 treatment (Zhou *et al.*, 2004). In addition, inhibition of GSK-3β in hippocampal neurons results in an ~1.9-fold increase in microtubule polymerization in the neuron shaft (Zhou *et al.*, 2004). Using analogous techniques in PC12 cells, we demonstrated that the fluorescence intensity of polymerized microtubules was increased (>1.75-fold) in PIPP RNAi neurite shafts, relative to that detected in scrambled RNAi control neurites (Figure 10). The observed hyperelongation of PIPP-deficient neurites therefore correlates with increased microtubule polymerization in the neurite shafts.

DISCUSSION

In the study reported here, we have characterized PIPP, revealing that the 5-phosphatase functions as a novel negative regulator of PI3-kinase-dependent neurite elongation. PIPP localizes predominantly to the neurite growth cone of PC12 cells undergoing differentiation. Overexpression of PIPP inhibits neurite elongation, whereas targeted depletion of PIPP leads to NGF-stimulated neurite hyperelongation. PIPP RNAi-mediated neurite hyperelongation was inhibited by low-dose wortmannin treatment, indicating this phenotype is dependent on PI3-kinase signaling. In differentiated neurites, increased phospho-Ser473-Akt staining at the growth cone, relative to the same neurite shaft, was detected in PIPP RNAi cells, correlating with increased PtdIns(3,4,5)P_3 and increased intensity of phospho-Ser9-GSK-3β/total GSK-3β at the growth cone, associated with increased microtubule polymerization in the neurite shaft. Therefore, PIPP may regulate PI3-kinase signaling specifically at the neurite growth cone, modulating neurite extension via the compartmentalized regulation of phospho-Ser473-Akt and phospho-Ser9-GSK-3β, despite the presence of global NGF stimulation.

The spatial-temporal control of the synthesis and/or hydrolysis of phosphoinositides on specific membranes is critical for the localized activation of downstream PI3-kinase-dependent signaling cascades. In dorsal root ganglion neurons, the PtdIns(3,4,5)P_3-effector phospho-Ser473-Akt localizes mainly in the cell body and the growth cone, but not the axon shaft (Zhou *et al.*, 2004). Phospho-Ser9-GSK-3β is also concentrated at the cell body and the distal end of the growth cone in hippocampal neurons (Jiang *et al.*, 2005). Studies in dorsal root ganglia have revealed that the inactivation of GSK-3β by PI3-kinase-dependent phosphorylation is critical for NGF-stimulated axon elongation (Zhou *et al.*, 2004). The activation of PI3-kinase selectively at the neurite growth cone produces PtdIns(3,4,5)P_3, facilitating Akt membrane recruitment, phosphorylation, and activation (Zhou *et al.*, 2004). Activated Akt, aPKC, and/or ILK phosphorylate and inhibit GSK-3β activity specifically at the growth cone. We propose that PIPP hydrolyzes PtdIns(3,4,5)P_3 at the growth cone, thereby decreasing Akt and GSK-3β phosphorylation at this site. In the absence of PIPP, sustained

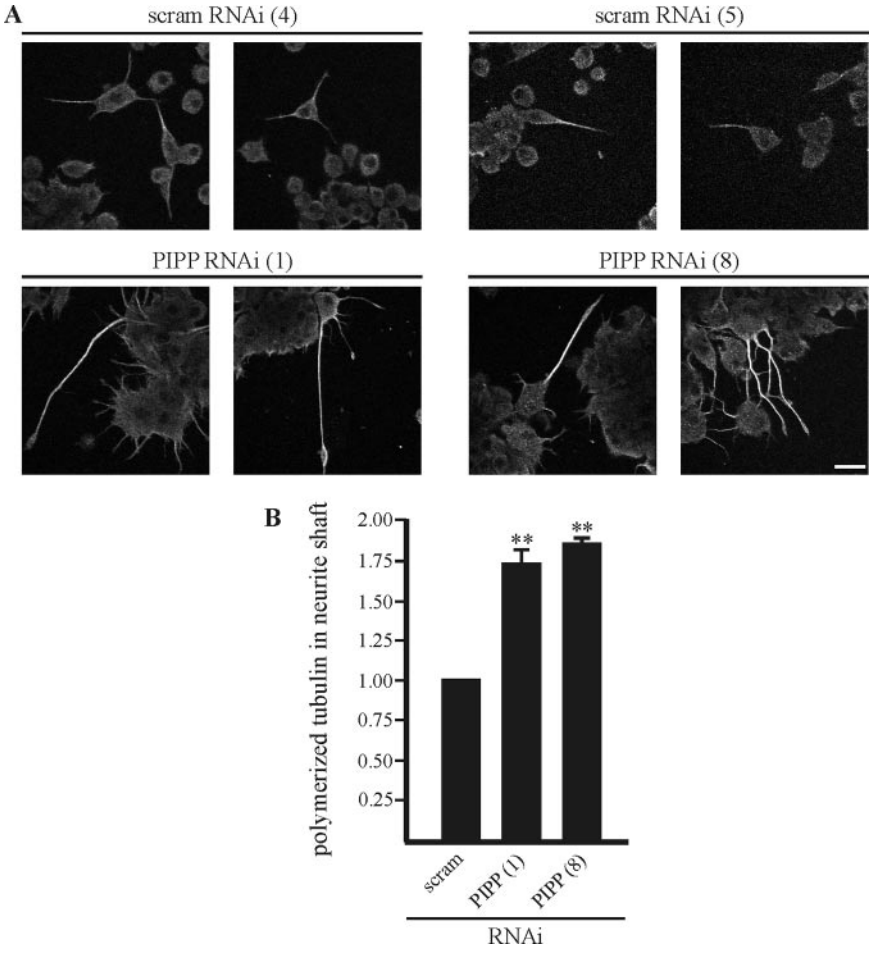

Figure 10. PIPP regulates microtubule polymerization. (A) NGF-differentiated neurites were fixed and extracted at the same time to eliminate free tubulin monomers, stained with β-tubulin antibodies, and imaged at the same laser attenuation. Representative images are shown. Scale bar, 20 μm. (B) Quantification of relative microtubule intensity at the neurite shaft. Bars represent the average fluorescence intensity within a 50 $\times$ 3-pixel box of the neurite shaft of >30 neurites per RNAi clone from two independent differentiation experiments, relative to that detected in scrambled clones, which is arbitrarily scored as 1 (** $p < 0.01$).

PtdIns(3,4,5)P_3-dependent growth cone signaling may lead to enhanced and/or sustained activation of Akt at the growth cone. The results of our studies suggest PIPP does not regulate the recruitment of Akt protein to the growth cone; rather, the 5-phosphatase regulates the activation of a pre-existing growth cone pool of Akt. Phospho-Ser473-Akt, but not total Akt protein, was increased at the growth cone relative to the neurite shaft after targeted depletion of PIPP. Similarly, the distribution and fluorescence intensity of the ratio of phospho-Ser9-GSK-3β/total GSK-3β at the growth cone was also increased in PIPP RNAi hyperelongated neurites, suggesting that PIPP does not promote the localization and/or recruitment of GSK-3β protein to the growth cone, but rather regulates the activation status of a preexisting growth-cone-GSK-3β pool. Because this kinase is not localized exclusively to the growth cone (Jiang *et al.*, 2005), the dissection of how the distinct spatial pools of GSK-3β function at the growth cone versus the cell body has not been comprehensively delineated. Recently published studies have shown that expression of constitutively activated/inactivated forms of Akt and GSK-3β show phenotypes similar to the effects of PIPP over- and underexpression. Studies by Jiang *et al.* (2005) have revealed that expression of constitutively-active Akt (myr-Akt) induces both multiple axon formation and in neurons where only one axon forms, hyperelongation of axons. Second, expression of constitutively active Akt (myr-Akt) in PC12 cells enhances the number of cells bearing neurites longer than two cell body diameters (Kim *et al.*, 2004). RNAi-mediated knock-down of GSK-3β in hippocampal neurons induces hyperelongation of neurons (Yoshimura *et al.*, 2005). In contrast, ectopic expression of wild-type GSK-3β or a mutant GSK-3β that cannot be phosphorylated at Ser9 and thereby be inactivated (GSK-3β S9A) inhibits axon elongation (Zhou *et al.*, 2004; Jiang *et al.*, 2005), reminiscent of the neurite phenotypes described here upon PIPP overexpression.

PIPP hydrolyzes PtdIns(4,5)P_2 in vitro (Mochizuki and Takenawa, 1999), although we were unable to demonstrate significant hydrolysis at the plasma membrane in intact cells. We have demonstrated here that PIPP also hydrolyzes PtdIns(3,4,5)P_3 forming PtdIns(3,4)P_2 and regulates the recruitment of PtdIns(3,4,5)P_3-binding PH domains to the plasma membrane of growth factor-stimulated COS-1 cells, inhibiting the amplitude of Ser473-Akt phosphorylation. PtdIns(4,5)P_2, a putative PIPP substrate, also may function as an inhibitory signal for neurite elongation and axonal branching. Expression of catalytically inactive type 1 PtdIns(4)P 5-kinase in hippocampal neurons promotes neuritogenesis (van Horck *et al.*, 2002; Yamazaki *et al.*, 2002), whereas its overexpression has no effect on axon length or branching (Hernandez-Deviez *et al.*, 2004). Coexpression of type 1 PtdIns(4)P 5-kinase with inactive ARNO or dominant negative ARF6, however, inhibits the increased neurite extension and branching observed in hippocampal neurons expressing either mutant alone, suggesting type 1 PtdIns(4)P 5-kinase/PtdIns(4,5)P_2 acts downstream of ARNO/ARF6 to restrict neurite elongation (Hernandez-Deviez *et al.*, 2004). PtdIns(4,5)P_2 may negatively affect axon extension by re-

cruiting various actin-binding proteins to the growth cone to regulate actin polymerization and remodeling (Yamazaki *et al.*, 2002; Hernandez-Deviez *et al.*, 2004). Interestingly, actin polymerization appeared relatively unchanged at the growth cone and neurite shaft of PIPP RNAi cells or cells overexpressing PIPP. Overexpression of PIPP inhibited neurite extension, without a requirement of coexpression of ARNO and/or ARF6. Furthermore, the PIPP RNAi-induced phenotype of neurite hyperelongation was rescued by low-dose wortmannin treatment. The weight of evidence suggests that PIPP regulates PtdIns(3,4,5)P_3 signaling and thereby neurite extension at the growth cone, rather than PtdIns(4,5)P_2-dependent signaling events. PtdIns(3,4,5)P_3 hydrolysis by PIPP generates the signal PtdIns(3,4)P_2. Recent studies have suggested PtdIns(3,4)P_2 may potentially play a role in neuronal development. Mice deficient in the type Iα inositol polyphosphate 4-phosphatase, which hydrolyzes PtdIns(3,4)P_2, accumulate this phosphoinositide and die in the neonatal period with cerebellar ataxia and growth retardation (Nystuen *et al.*, 2001; Ivetac *et al.*, 2005; Shin *et al.*, 2005). PtdIns(3,4)P_2 is a signaling molecule in its own right, which recruits effector proteins to the plasma membrane and although the role this phosphoinositide plays in axon elongation remains unexplored, we cannot exclude the possibility that altered levels of PtdIns(3,4)P_2, at least in part, contributes to the observed neurite phenotypes that were detected upon PIPP over- or underexpression.

Axon elongation is dependent on microtubule polymerization (reviewed Cleveland and Hoffman, 1991). Recently, it has been proposed that the GSK-3β/APC pathway is critical for NGF-stimulated microtubule dynamics that promote axon elongation, independent of actin dynamics (Zhou *et al.*, 2004). Targeted depletion of PIPP results in increased microtubule polymerization, correlating with neurite hyperelongation, but no apparent change in actin polymerization in the developing neurite shaft or growth cone. PIPP does not localize to the early developing neurite actin-rich spike or to the actin-rich neurite tip of differentiated neurites, and this may in part explain why its overexpression or targeted depletion does not regulate neurite initiation or actin polymerization. Ectopically expressed recombinant PIPP localizes to membrane ruffles, colocalizing with active Rac1; however, its overexpression has no overt effect on actin dynamics (Mochizuki and Takenawa, 1999). Our results suggest that PIPP regulates neurite elongation via indirect regulation of the spatial stabilization and/or polymerization of microtubules, rather than via any direct effect on actin dynamics. Collectively this study suggests PIPP functions at the growth cone in PC12 cells and via hydrolysis of its cognate substrate PtdIns(3,4,5)P_3 functions at this site as a regulator of Akt/GSK-3β-dependent signaling, microtubule polymerization, and thereby neurite elongation.

ACKNOWLEDGMENTS

This work was supported by a Cancer Council of Victoria grant. Imaging was performed at Monash University Imaging Facility.

REFERENCES

Abramoff, M., Magelhaes, P., and Ram, S. (2004). Image processing with Image J. Biophotonics Int. *11*, 36–42.

Aoki, K., Nakamura, T., and Matsuda, M. (2004). Spatio-temporal regulation of Rac1 and Cdc42 activity during nerve growth factor-induced neurite outgrowth in PC12 Cells. J. Biol. Chem. *279*, 713–719.

Baas, P. W., and Luo, L. (2001). Signaling at the growth cone: the scientific progeny of Cajal meet in Madrid. Neuron *32*, 981–984.

Balla, T., Bondeva, T., and Varnai, P. (2000). How accurately can we image inositol lipids in living cells? Trends Pharmacol. Sci. *21*, 238–241.

Bang, O. S., Park, E. K., Yang, S. I., Lee, S. R., Franke, T. F., and Kang, S. S. (2001). Overexpression of Akt inhibits NGF-induced growth arrest and neuronal differentiation of PC12 cells. J. Cell Sci. *114*, 81–88.

Bernstein, M., and Lichtman, J. W. (1999). Axonal atrophy: the retraction reaction. Curr. Opin. Neurobiol. *9*, 364–370.

Cantley, L. C. (2002). The phosphoinositide 3-kinase pathway. Science *296*, 1655–1657.

Carter, A. N., and Downes, C. P. (1992). Phosphatidylinositol 3-kinase is activated by nerve growth factor and epidermal growth factor in PC12 cells. J. Biol. Chem. *267*, 14563–14567.

Cho, J.-H., and Johnson, G.V.W. (2004). Primed phosphorylation of tau at Thr231 by glycogen synthase kinase 3β (GSK-3β) plays a critical role in regulating tau's ability to bind and stabilize microtubules. J. Neurochem. *88*, 349–358.

Clement, S. *et al.* (2001). The lipid phosphatase SHIP2 controls insulin sensitivity. Nature *409*, 92–97.

Cleveland, D. W., and Hoffman, P. N. (1991). Neuronal and glial cytoskeletons. Curr. Opin. Neurobiol. *1*, 346–353.

Cremona, O., Di Paolo, G., Wenk, M. R., Luthi, A., Kim, W. T., Takei, K., Daniell, L., Nemoto, Y., Shears, S. B., and Flavell, R. A. (1999). Essential role of phosphoinositide metabolism in synaptic vesicle recycling. Cell *99*, 179–188.

Cross, D. A., Alessi, D. R., Cohen, P., Andjelkovich, M., and Hemmings, B. A. (1995). Inhibition of glycogen synthase kinase-3 by insulin mediated by protein kinase B. Nature *378*, 785–789.

Dickson, B. J. (2002). Molecular mechanisms of axon guidance. Science *298*, 1959–1964.

Dyson, J. M., O'Malley, C. J., Becanovic, J., Munday, A. D., Berndt, M. C., Coghill, I. D., Nandurkar, H. H., Ooms, L. M., and Mitchell, C. A. (2001). The SH2-containing inositol polyphosphate 5-phosphatase, SHIP-2, binds filamin and regulates submembraneous actin. J. Cell Biol. *155*, 1065–1079.

Franke, T. F., Kaplan, D. R., Cantley, L. C., and Toker, A. (1997). Direct regulation of the Akt proto-oncogene product by phosphatidylinositol-3,4-bisphosphate. Science *275*, 665–668.

Freeburn, R. W., Wright, K. L., Burgess, S. J., Astoul, E., Cantrell, D. A., and Ward, S. G. (2002). Evidence that SHIP-1 contributes to phosphatidylinositol 3,4,5-trisphosphate metabolism in T lymphocytes and can regulate novel phosphoinositide 3-kinase effectors. J. Immunol. *169*, 5441–5450.

Gallo, G., and Letourneau, P. C. (1998). Localized sources of neurotrophins initiate axon collateral sprouting. J. Neurosci. *18*, 5403–5414.

Goold, R. G., Owen, R., and Gordon-Weeks, P. R. (1999). Glycogen synthase kinase 3β phosphorylation of microtubule-associated protein 1B regulates the stability of microtubules in growth cones. J. Cell Sci. *112*, 3373–3384.

Gordon-Weeks, P. R. (1991). Growth cones: the mechanism of neurite advance. Bioessays *13*, 235–239.

Greene, L.A., and Tischler, A. S. (1976). Establishment of a noradrenergic clonal line of rat adrenal pheochromocytoma cells which respond to nerve growth factor. Proc. Natl. Acad. Sci. USA *73*, 2424–2428.

Gurung, R., Tan, A., Ooms, L. M., McGrath, M. J., Huysmans, R. D., Munday, A. D., Prescott, M., Whisstock, J. C., and Mitchell, C. A. (2003). Identification of a novel domain in two mammalian inositol-polyphosphate 5-phosphatases that mediates membrane ruffle localization. The inositol 5-phosphatase SKIP localizes to the endoplasmic reticulum and translocates to membrane ruffles following epidermal growth factor stimulation. J. Biol. Chem. *278*, 11376–11385.

Halegoua, S., Armstrong, R. C., and Kremer, N. E. (1991). Dissecting the mode of action of a neuronal growth factor. Curr. Top. Microbiol. Immunol. *165*, 119–170.

Hall, A. C., Brennan, A., Goold, R. G., Cleverley, K., Lucas, F. R., Gordon-Weeks, P. R., and Salinas, P. C. (2002). Valproate regulates GSK-3-mediated axonal remodeling and synapsin I clustering in developing neurons. Mol. Cell. Neurosci. *20*, 257–270.

He, Y., Yu, W., and Baas, P. W. (2002). Microtubule reconfiguration during axonal retraction induced by nitric oxide. J. Neurosci. *22*, 5982–5991.

Helgason, C. D., Damen, J. E., Rosten, P., Grewal, R., Sorensen, P., Chappel, S. M., Borowski, A., Jirik, F., Krystal, G., and Humphries, R. K. (1998). Targeted disruption of SHIP leads to hemopoietic perturbations, lung pathology, and a shortened life span. Genes Dev. *12*, 1610–1620.

Hellsten, E., Bernard, D. J., Owens, J. W., Eckhaus, M., Suchy, S. F., and Nussbaum, R. L. (2002). Sertoli cell vacuolization and abnormal germ cell

adhesion in mice deficient in an inositol polyphosphate 5-phosphatase. Biol. Reprod. *66*, 1522–1530.

Hernandez-Deviez, D. J., Roth, M. G., Casanova, J. E., and Wilson, J. M. (2004). ARNO and ARF6 regulate axonal elongation and branching through downstream activation of phosphatidylinositol 4-phosphate 5-kinase α. Mol. Biol. Cell *15*, 111–120.

Higuchi, M., Onishi, K., Masuyama, N., and Gotoh, Y. (2003). The phosphatidylinositol-3 kinase (PI3K)-Akt pathway suppresses neurite branch formation in NGF-treated PC12 cells. Genes Cells *8*, 657–669.

Ijuin, T., and Takenawa, T. (2003). SKIP negatively regulates insulin-induced GLUT4 translocation and membrane ruffle formation. Mol. Cell. Biol. *23*, 1209–1220.

Ivetac, I., Munday, A. D., Kisseleva, M. V., Zhang, X.-M., Luff, S., Tiganis, T., Whisstock, J. C., Rowe, T., Majerus, P. W., and Mitchell, C. A. (2005). The type Iα inositol polyphosphate 4-phosphatase generates and terminates phosphoinositide 3-kinase signals on endosomes and the plasma membrane. Mol. Biol. Cell *16*, 2218–2233.

Jackson, T. R., Blader, I. J., Hammonds-Odie, L. P., Burga, C. R., Cooke, F., Hawkins, P. T., Wolf, A. G., Heldman, K. A., and Theibert, A. B. (1996). Initiation and maintenance of NGF-stimulated neurite outgrowth requires activation of a phosphoinositide 3-kinase. J. Cell Sci. *109*, 289–300.

Jiang, H., Guo, W., Liang, X., and Rao, Y. (2005). Both the establishment and the maintenance of neuronal polarity require active mechanisms: critical roles of GSK-3β and its upstream regulators. Cell *120*, 123–135.

Jones, D. M., Tucker, B. A., Rahimtula, M., and Mearow, K. M. (2003). The synergistic effects of NGF and IGF-1 on neurite growth in adult sensory neurons: convergence on the PI 3-kinase signaling pathway. J. Neurochem. *86*, 1116–1128.

Kim, C., Hangoc, G., Cooper, S., Helgason, C. D., Yew, S., Humphries, R. K., Krystal, G., and Broxmeyer, H. E. (1999). Altered responsiveness to chemokines due to targeted disruption of SHIP. J. Clin. Invest. *104*, 1751–1759.

Kim, Y., Seger, R., Babu, S., Hwang, S., and Sook Yoo, Y. (2004). A positive role of the PI3-K/Akt signaling pathway in PC12 cell differentiation. Mol. Cell *18*, 353–359.

Kimura, K., Hattori, S., Kabuyama, Y., Shizawa, Y., Takayanagi, J., Nakamura, S., Toki, S., Matsuda, Y., Onodera, K., and Fukui, Y. (1994). Neurite outgrowth of PC12 cells is suppressed by wortmannin, a specific inhibitor of phosphatidylinositol 3-kinase. J. Biol. Chem. *269*, 18961–18967.

Kisseleva, M. V., Cao, L., and Majerus, P. W. (2002). Phosphoinositide-specific inositol polyphosphate 5-phosphatase IV inhibits Akt/Protein Kinase B phosphorylation and leads to apoptotic cell death. J. Biol. Chem. *277*, 6266–6272.

Kobayashi, M. *et al.* (1997). Expression of a constitutively active phosphatidylinositol 3-kinase induces process formation in rat PC12 cells. Use of Cre/loxP recombination system. J. Biol. Chem. *272*, 16089–16092.

Kong, A. M., Speed, C. J., O'Malley, C. J., Layton, M. J., Meehan, T., Loveland, K. L., Cheema, S., Ooms, L. M., and Mitchell, C. A. (2000). Cloning and characterization of a 72-kDa inositol-polyphosphate 5-phosphatase localized to the Golgi network. J. Biol. Chem. *275*, 24052–24064.

Lee, H., and Van Vactor, D. (2003). Neurons take shape. Curr. Biol. *13*, R152–R161.

Mills, J., Digicaylioglu, M., Legg, A. T., Young, C. E., Young, S. S., Barr, A. M., Fletcher, L., O'Connor, T. P., and Dedhar, S. (2003). Role of integrin-linked kinase in nerve growth factor-stimulated neurite outgrowth. J. Neurosci. *23*, 1638–1648.

Ming, G.-L., Song, H.-J., Berninger, B., Inagaki, N., Tessier-Lavigne, M., and Poo, M.-M. (1999). Phospholipase C-γ and phosphoinositide 3-kinase mediate cytoplasmic signaling in nerve growth cone guidance. Neuron *23*, 139–148.

Mitchell, C. A., Gurung, R., Kong, A. M., Dyson, J. M., Tan, A., and Ooms, L. M. (2002). Inositol polyphosphate 5-phosphatases: lipid phosphatases with flair. IUBMB Life *53*, 25–36.

Mochizuki, Y., and Takenawa, T. (1999). Novel inositol polyphosphate 5-phosphatase localizes at membrane ruffles. J. Biol. Chem. *274*, 36790–36795.

Murakami, S., Sasaoka, T., Wada, T., Fukui, K., Nagira, K., Ishihara, H., Usui, I., and Kobayashi, M. (2004). Impact of Src Homology 2-containing inositol 5′-phosphatase 2 on the regulation of insulin signaling leading to protein synthesis in 3T3–L1 adipocytes cultured with excess amino acids. Endocrinology *145*, 3215–3223.

Nystuen, A., Legare, M. E., Shultz, L. D., and Frankel, W. N. (2001). A null mutation in inositol polyphosphate 4-phosphatase type I causes selective neuronal loss in Weeble mutant mice. Neuron *32*, 203–212.

Oatey, P. B., Venkateswarlu, K., Williams, A. G., Fletcher, L. M., Foulstone, E. J., Cullen, P. J., and Tavare, J. M. (1999). Confocal imaging of the subcellular distribution of phosphatidylinositol 3,4,5-trisphosphate in insulin- and platelet-derived growth factor-stimulated 3T3–L1 adipocytes. Biochem. J. 344 Pt *2*, 511–518.

Paves, H., Neuman, T., Metsis, M., and Saarma, M. (1988). Nerve growth factor induces rapid redistribution of F-actin in PC12 cells. FEBS Lett. *235*, 141–143.

Raffioni, S., and Bradshaw, R. (1992). Activation of phosphatidylinositol 3-kinase by epidermal growth factor, basic fibroblast growth factor, and nerve growth factor in PC12 pheochromocytoma cells. Proc. Natl. Acad. Sci. USA *89*, 9121–9125.

Rodgers, E. E., and Theibert, A. B. (2002). Functions of PI 3-kinase in development of the nervous system. Int. J. Dev. Neurosci. *20*, 187–197.

Sasaoka, T., Wada, T., Fukui, K., Murakami, S., Ishihara, H., Suzuki, R., Tobe, K., Kadowaki, T., and Kobayashi, M. (2004). SH2-containing inositol phosphatase 2 predominantly regulates Akt2, and not Akt1, phosphorylation at the plasma membrane in response to insulin in 3T3–L1 adipocytes. J. Biol. Chem. *279*, 14835–14843.

Scheid, M. P., Huber, M., Damen, J. E., Hughes, M., Kang, V., Neilsen, P., Prestwich, G. D., Krystal, G., and Duronio, V. (2002). Phosphatidylinositol (3,4,5)P_3 is essential but not sufficient for protein kinase B (PKB) activation; phosphatidylinositol (3,4)P_2 is required for PKB phosphorylation at Ser-473. Studies using cells from SH2-containing inositol-5-phosphatase knockout mice. J. Biol. Chem. *277*, 9027–9035.

Shi, S. H., Jan, L. Y., and Jan, Y. N. (2003). Hippocampal neuronal polarity specified by spatially localized mPar3/mPar6 and PI 3-kinase activity. Cell *112*, 63–75.

Shin, H.-W. *et al.* (2005). An enzymatic cascade of Rab5 effectors regulates phosphoinositide turnover in the endocytic pathway. J. Cell Biol. *170*, 607–618.

Skaper, S. D., Moore, S. E., and Walsh, F. S. (2001). Cell signalling cascades regulating neuronal growth-promoting and inhibitory cues. Prog. Neurobiol. *65*, 593–608.

Sleeman, M. W. *et al.* (2005). Absence of the lipid phosphatase SHIP2 confers resistance to dietary obesity. Nat. Med. *11*, 199–205.

Soltoff, S., Rabin, S., Cantley, L., and Kaplan, D. (1992). Nerve growth factor promotes the activation of phosphatidylinositol 3- kinase and its association with the trk tyrosine kinase. J. Biol. Chem. *267*, 17472–17477.

Tanaka, E., and Sabry, J. (1995). Making the connection: cytoskeletal rearrangements during growth cone guidance. Cell *83*, 171–176.

van Horck, F.P.G., Lavazais, E., Eickholt, B. J., Moolenaar, W. H., and Divecha, N. (2002). Essential role of Type Iα phosphatidylinositol 4-phosphate 5-kinase in neurite remodeling. Curr. Biol. *12*, 241–245.

Whisstock, J. C., Romero, S., Gurung, R., Nandurkar, H., Ooms, L. M., Bottomley, S. P., and Mitchell, C. A. (2000). The inositol polyphosphate 5-phosphatases and the Apurinic/Apyrimidinic base excision repair endonucleases share a common mechanism for catalysis. J. Biol. Chem. *275*, 37055–37061.

Yamazaki, M., Miyazaki, H., Watanabe, H., Sasaki, T., Maehama, T., Frohman, M. A., and Kanaho, Y. (2002). Phosphatidylinositol 4-phosphate 5-kinase is essential for ROCK-mediated neurite remodeling. J. Biol. Chem. *277*, 17226–17230.

Yoshimura, T., Kawano, Y., Arimura, N., Kawabata, S., Kikuchi, A., and Kaibuchi, K. (2005). GSK-3β regulates phosphorylation of CRMP-2 and neuronal polarity. Cell *120*, 137–149.

Zhou, F.-Q., and Snider, W. D. (2005). Cell Biology: GSK-3β and microtubule assembly in axons. Science *308*, 211–214.

Zhou, F.-Q., Zhou, J., Dedhar, S., Wu, Y.-H., and Snider, W. D. (2004). NGF-induced axon growth is mediated by localized inactivation of GSK-3β and functions of the microtubule plus end binding protein APC. Neuron *42*, 897–912.

Zumbrunn, J., Kinoshita, K., Hyman, A. A., and Nathke, I. S. (2001). Binding of the adenomatous polyposis coli protein to microtubules increases microtubule stability and is regulated by GSK3 beta phosphorylation. Curr. Biol. *11*, 44–49.